Nano Research

ISSN 1998-0124 CN 11-5974/O4
https://doi.org/10.26599/NR.2026.94908889

Review Article

# Flexible multifunctional MXene/nanocellulose nanocomposites for mechanical and electromagnetic shielding performance

Qi Liu[1,§], Jia-Qi Lang[1,§], Lei Chen[1,§], Chuanyin Xiong[2](✉), Xiufu Hua[3,4](✉), Ming-Guo Ma[1](✉)

[1] MOE Engineering Research Center of Forestry Biomass Materials and Bioenergy, Research Center of Biomass Clean Utilization, College of Materials Science and Technology, Beijing Forestry University, Beijing 100083, China

[2] College of Bioresources Chemical & Materials Engineering, Shaanxi University of Science and Technology, Xi'an 710021, China

[3] Institute of Low-Carbon Technology Application, School of Chemical and Engineering, Northwest University, Xi'an 710069, China

[4] Yangtze Delta Region Institute, Tsinghua University, Jiaxing 314006, China

[§] Qi Liu, Jia-Qi Lang, and Lei Chen contributed equally to this work.

*Nano Res.*, **Just Accepted Manuscript** • https://doi.org/10.26599/NR.2026.94908889

**https://www.sciopen.com/journal/1998-0124** on May. 27, 2026

*Table of Contents*

# Flexible multifunctional MXene/nanocellulose nanocomposites for mechanical and electromagnetic shielding performance

Qi Liu,[a,1] Jia-Qi Lang,[a,1] Lei Chen,[a,1] Chuanyin Xiong,[b*] Xiufu Hua,[c,d*] Ming-Guo Ma[a,*]

[a]MOE Engineering Research Center of Forestry Biomass Materials and Bioenergy, Research Center of Biomass Clean Utilization, College of Materials Science and Technology, Beijing Forestry University, Beijing 100083, PR China;

[b]College of Bioresources Chemical & Materials Engineering, Shaanxi University of Science and Technology, Xi'an 710021, PR China;

[c]Institute of Low-Carbon Technology Application, School of Chemical and Engineering, Northwest University, Xi'an 710069, PR China;

[d]Yangtze Delta Region Institute, Tsinghua University, Jiaxing 314006, PR China.




* Corresponding author. Tel.: +0086-10-62337250. E-mail address: mg_ma@bjfu.edu.cn (M.-G. Ma), huaxf@nwu.edu.cn (X.-F. Hua), xiongchuanyin@126.com (C.-Y. Xiong).

[1]Qi Liu, Jia-Qi Lang, and Lei Chen contributed equally to this work.

**Review Article**

# Flexible multifunctional MXene/nanocellulose nanocomposites for mechanical and electromagnetic shielding performance

Qi Liu,[1, §] Jia-Qi Lang,[1, §] Lei Chen,[1, §] Chuanyin Xiong,[2*] Xiufu Hua,[3,4*] and Ming-Guo Ma[1,*]

[1]MOE Engineering Research Center of Forestry Biomass Materials and Bioenergy, Research Center of Biomass Clean Utilization, College of Materials Science and Technology, Beijing Forestry University, Beijing 100083, China

[2]College of Bioresources Chemical & Materials Engineering, Shaanxi University of Science and Technology, Xi'an 710021, China

[3]Institute of Low-Carbon Technology Application, School of Chemical and Engineering, Northwest University, Xi'an 710069, China

[4]Yangtze Delta Region Institute, Tsinghua University, Jiaxing 314006, China

[§]Qi Liu, Jia-Qi Lang, and Lei Chen contributed equally to this work.

Received: 26 April 2026; Revised: 27 May 2026; Accepted: 27 May 2026

*Address correspondence to Ming-Guo Ma, mg_ma@bjfu.edu.cn; Xiufu Hua, huaxf@nwu.edu.cn; Chuanyin Xiong, xiongchuanyin@126.com

Cite this article: Nano Research, 2026, 19, 94908889 https://doi.org/10.26599/NR.2026.94908889

**Abstract**

In recent decades, electromagnetic shielding materials have been widely explored due to their promising applications in electronic communication, aerospace, military, and medical equipment. Numerous pioneering works have been reported on MXene/nanocellulose composites, which possess various structures and excellent electromagnetic shielding properties. This article reviews the latest progress of MXene/nanocellulose composites in electromagnetic interface shielding applications, with a particular focus on preparation strategies, toughening mechanisms, and structural design. More importantly, we have reviewed the toughening mechanism of MXene/nanocellulose composites from three aspects: physical toughening mechanism, chemical toughening mechanism, and synergistic toughening mechanism. In addition, we systematically analyzed the current technological limitations and proposed potential research directions to guide future development. This work will greatly advance the rational design and practical application of high-performance MXene/nanocellulose electromagnetic shielding composites.

**Keywords:** MXene, nanocellulose, composites, electromagnetic shielding, preparation strategies, toughening mechanism

**List of Abbreviations**

| | |
|---|---|
| **0D** | Zero-dimensional |
| **1D** | One-dimensional |
| **2D** | Two-dimensional |
| **3D** | Three-dimensional |
| **AgNPs** | Silver nanoparticles |
| **AgNWs** | Silver nanowires |
| **BNC** | Bacterial nanocellulose |
| **CNC** | Cellulose nanocrystal |
| **CNF** | Cellulose nanofiber |
| **CVD** | Chemical vapor deposition |
| **EMI** | Electromagnetic interference |
| **GO** | Graphene oxide |
| **HF** | Hydrofluoric acid |
| **MFC** | Micro-fibrillated cellulose |
| **PDA** | Polydopamine |
| **PVD** | Physical vapor deposition |
| **SE** | Shielding effectiveness |
| **CMC** | Carboxymethyl cellulose |
| **LM** | Liquid metal |
| **PCNF** | Phosphorylated cellulose nanofibrils |
| **APD** | Ambient-pressure drying |
| **MMAs** | Magnetic MXene aerogels |
| **PAAm** | Polyacrylamide |
| **TA** | Tannic acid |
| **PDMS** | Polydimethylsiloxanes |
| **PMDI** | Poly((phenylisocyanate)-co-formaldehyde) |
| **ANF** | Aramid nanofiber |
| **AVF** | Alternating vacuum filtration |
| **LBL** | Layer-by-layer |
| **MCHS** | Mesoporous carbon hollow spheres |
| **MOFs** | Metal-organic frameworks |
| **PAA** | Polyacrylic acid |
| **TENG** | Triboelectric nanogenerator |
| **ZIF** | Zeolitic imidazolate framework |
| **rGO** | Reduced graphene oxide |
| **BC** | Bacterial cellulose |
| **PPy** | Polypyrrole |
| **MS** | MXene $Ti_3C_2T_x$ sediment |
| **SA** | Sodium alginate |
| **TPU** | Thermoplastic polyurethane |
| **BNNS** | Boron nitride nanoplates |
| **EMI SE** | Electromagnetic interface shielding effectiveness |

## 1 Introduction

Electromagnetic shielding materials block the propagation of electromagnetic waves through mechanisms, such as reflection, refraction, which have important application prospects in fields of electronic communication, aerospace, military, and medical equipment [1,2]. However, traditional electromagnetic shielding materials (e.g., metallic materials, conductive polymers, and carbon-based materials) often face limitations such as high weight, poor flexibility, or high cost [2,3].

In recent years, researchers have developed a variety of new electromagnetic shielding materials to overcome these limitations, including MOFs, carbon nanotube/graphene hybrids, and two-dimensional transition metal carbides/nitrides (MXenes) [4]. These emerging materials have enabled diverse structural design strategies—such as porous architectures, multilayer assemblies, and core‑shell structures—that enhance electromagnetic wave attenuation through tailored impedance matching and multiple internal reflections. Among these materials, MXenes have attracted attention due to their excellent performance, with a unique layered structure and excellent electrical conductivity, thermal conductivity, and chemical stability [5]. MXenes have shown great potential in the field of electromagnetic shielding, as they can effectively reflect and absorb electromagnetic waves [6]. As early as 2016, Gogotsi *et al.* [7] developed a highly flexible MXene composite film with a thickness of only 45 μm, which can block 99.99% of incident radiation and achieve a SE of -92 dB, comparable to traditional metal shielding materials. It provides a new approach to solving EMI problems with excellent electromagnetic shielding performance. Then, they found that MXene ($Ti_3CNT_x$) thin composite films with a thickness of only 55 μm and moderate conductivity exhibited excellent electromagnetic shielding performance.

They could effectively reflect electromagnetic waves and absorb electromagnetic radiation, thereby reducing EMI and avoiding the secondary reflection problem that traditional metal shielding materials may cause [8]. MXene thin composite film with 55 μm and moderate conductivity exhibited excellent EMI SE, breaking the limitations of traditional understanding. More recently, Zhang *et al.* [9] proposed a theoretical model for insulating electromagnetic shielding structures, adopting the strategies of "non-percolation densification" and "dielectric optimization" to achieve the integration of high electrical insulation and excellent electromagnetic shielding performance in silicone rubber/LM composite systems. This study provides a new technological approach to address electromagnetic compatibility and efficient heat dissipation issues in highly integrated electronic packaging [10].

The development of EMI shielding materials has evolved from conventional metals (high conductivity but heavy and inflexible) to conductive polymer composites and carbon-based materials (lighter and flexible but costly and prone to agglomeration). In this context, MXene/polymer composites combine the metallic conductivity of MXene with polymer processability, emerging as highly efficient EMI shields. Recent reviews have summarized the fabrication strategies and structural design principles of MXene‐based composites, highlighting how porous structures, multilayer architectures, and magnetic‐dielectric synergy enable absorption‐dominant shielding [11]. Beyond pure EMI shielding, MXene-based materials are also extensively explored for microwave absorption [12]. Shafiee *et al.* [13] systematically reviewed MXene‐based metal oxide/metal composites for this purpose, emphasizing the role of metal/metal oxide nanoparticles in introducing magnetic loss and improving impedance matching. Morphology, phase composition, and defect engineering further enhance microwave attenuation

through synergistic dielectric- magnetic loss mechanisms [14]. These insights are valuable for designing MXene/nanocellulose composites with balanced shielding and absorption properties.

To rationally design high-performance MXene/nanocellulose composites, it is essential to understand the trade-offs among fabrication methods, morphological characteristics, and the resulting mechanical and EMI shielding properties [15]. Vacuum-assisted filtration yields highly conductive, layered composite films with exceptional shielding efficiency; however, scalability remains a challenge. Freeze-drying produces ultralight, porous aerogels that achieve absorption-dominated shielding, yet these structures often suffer from suboptimal mechanical strength. Alternatively, 3D printing enables customizable, gradient architectures, whereas wet spinning can produce continuous fibers with excellent flexibility but relatively low electrical conductivity. The morphology of the material—whether 1D fibers, 2D composite films, or 3D networks—dictates the underlying shielding mechanism [16]. While 2D layered structures favor reflection due to their dense, conductive networks [17], 3D porous structures promote multiple internal scattering and absorption, although increasing porosity inherently compromises mechanical strength [18]. Beyond morphology, phase composition, doping, and defects significantly modulate microwave absorption performance. Introducing a magnetic phase (such as $Fe_3O_4$) creates a magneto-dielectric synergistic effect, heteroatom doping induces dipole polarization, and controllable defects serve as polarization centers [19]. While these strategies enhance absorption, they may do so at the expense of electrical conductivity and strength. Furthermore, the choice of MXene synthesis route (HF etching versus greener molten-salt or electrochemical etching) and the nanocellulose source (wood-derived CNFs, bacterial cellulose, or TEMPO-oxidized CNFs) directly influences flake size, defect density, and surface chemistry,

ultimately determining the mechanical and shielding properties of the composites. Consequently, achieving an optimal balance necessitates an integrated design that comprehensively orchestrates MXene synthesis, cellulose selection, and assembly strategies.

MXene/nanocellulose composites combine the lightweight, high specific surface area, and good flexibility of nanocellulose with the excellent conductivity of MXene [20,21]. Nanocellulose can provide mechanical support [22], while MXene nanosheets effectively reflect and absorb electromagnetic waves through their 2D layered structure and high conductivity [23], thereby achieving efficient electromagnetic shielding effects [24]. This composite is suitable for electromagnetic shielding applications in electronic device casings, flexible electronic devices, wearable devices, and aerospace [25]. More recently, Cheng *et al.* [26] proposed a new strategy of "LM cross-linking densification" to prepare the MXene/LM/BC nanocomposite composite film with the highest tensile strength to date, which also exhibited excellent electromagnetic shielding performance. In previous review article, we summarized the design strategies of MXene/nanocellulose composites and their diverse applications in electromagnetic shielding, energy storage, environmental remediation, and biomedical fields [27]. However, there are few detailed reports and comparisons on the preparation strategies, toughening mechanisms, and structural design of MXene/nanocellulose composites for EMI shielding applications.

Several review articles also have recently addressed MXene- based composites for EMI shielding. However, to the best of our knowledge, no existing review simultaneously integrates three critical aspects: a comprehensive comparison of preparation strategies with explicit evaluation of their trade- offs in mechanical and shielding performance, a detailed mechanistic analysis of toughening mechanisms (physical, chemical, and synergistic), and a systematic

comparative framework of multidimensional structural designs (1D fibers, 2D composite films, and 3D foams/aerogels/hydrogels). This review fills this gap by providing a holistic perspective that connects fabrication methods, toughening mechanisms, and structural architectures, offering readers a comprehensive understanding of how to design MXene/nanocellulose composites with optimized mechanical and electromagnetic performance.

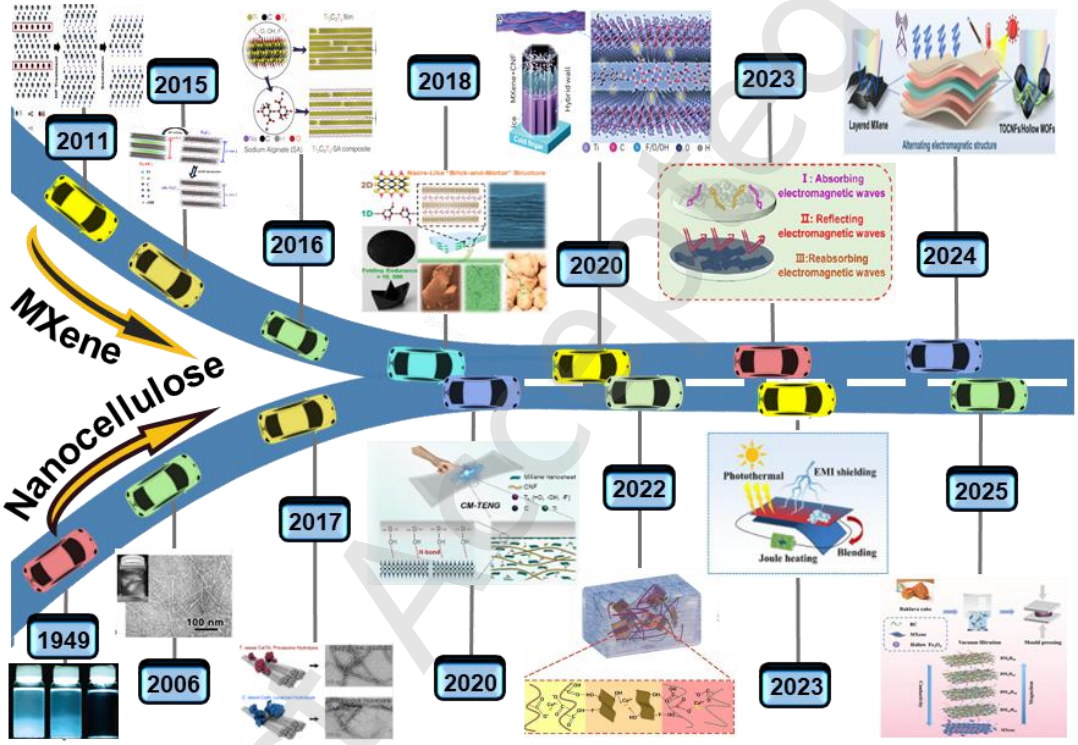


**Figure 1** The development of MXene/nanocellulose EMI shielding composites from fundamental research to multifunctional integration in recent years. Rånby (1949): First colloidal CNC report. Reproduced with permission from Ref. [28], © American Chemical Society 2007. 2006: Isogai's TEMPO-oxidation for CNF. [29], © 2006 American Chemical Society. Gogotsi (2011): $Ti_3C_2T_x$ MXene synthesis. Reproduced with permission from Ref. [30], © WILEY‐VCH Verlag GmbH & Co. KGaA, Weinheim 2011. Zhu (2015): alkaline intercalation of $Ti_3C_2$. MXene Reproduced with permission from Ref. [31], © Elsevier Ltd. 2017. Yarbrough (2017): multifunctional cellulases enable stable coproduction. Reproduced with permission from Ref. [32], © American Chemical Society 2017. Shahzad (2016): MXene superior EMI shielding. Reproduced with permission from Ref. [7], © The American Association for the Advancement of Science 2016. Ma (2018): MXene/CNF synergy (65 dB). Reproduced with permission from Ref. [33], © Cao, W. T. et al. 2018. Ma (2020): MXene/nanocellulose TENG sensors. Reproduced with permission from [34], © Wiley‐VCH GmbH 2020. Zeng (2020): Biomimetic EMI shielding aerogels.

Reproduced with permission from [35], © Zeng, Z. H. et al., WILEY‐VCH Verlag GmbH & Co. KGaA, Weinheim 2020. Zeng (2022): Functional shielding hydrogels. Reproduced with permission from [36], © Zeng, Z. H. et al., Interdisciplinary Materials published by Wuhan University of Technology and John Wiley & Sons Australia, Ltd 2022. Mai (2023): C-ZIF/MXene/CNF absorption-dominant paper. Reproduced with permission from [37], © Mai, T. et al 2024. He (2023): Nacre-inspired CNF/MXene@Ga composite film. Reproduced with permission from [38], © Elsevier B.V. 2023. Mai (2024): Hollow MOF/MXene/CNF shielding-photothermal composite film. Reproduced with permission from [39], © Mai, T. et al 2024. Pan (2025): Dual-gradient BC/MXene/HFO composite film (67.6 dB) with Joule heating & IR camouflage. Reproduced with permission from Ref. [40], © Wiley‐VCH GmbH 2025.

**Figure 1** illustrates the development of MXene and nanocellulose in the field of electromagnetic shielding materials. These advanced materials gradually improved their performance in electromagnetic wave absorption and shielding. The current research trend indicates that the applications of these composites in the field of electromagnetic protection will become increasingly diverse, especially in emerging fields that require flexible, lightweight, and multifunctional shielding solutions. In this review, the recent developments of MXene/nanocellulose composites in EMI shielding are summarized. The preparation strategies of MXene/nanocellulose composites are also introduced. Moreover, the toughening mechanism and structural design of MXene/nanocellulose composites are described in detail. Finally, based on our knowledge, the current challenges and future directions are also proposed.



## 2 Preparation strategies of MXene/nanocellulose composites

Using the complementary structure and chemical properties of MXene and nanocellulose, multidimensional MXene/nanocellulose composites have been fabricated in various structures, including fibers, composite films, hydrogels, aerogels, and foams [41]. The synthesis of MXene mainly involves two different strategies, including "top-down" and "bottom-up" approaches [42].

Currently, acid etching method dominates in practical applications, while alternative methods such as electrochemical etching, alkaline etching, and molten salt etching show considerable developmental prospects. Amara *et al.* [43] have pioneered an innovative HF direct etching method for the synthesis of MXene, including $Ti_3C_2$, $Ti_2C$, and $Ta_4C_3$. Excessive etching conditions may lead to an increase in crystal defects and even structural collapse. The improvements greatly reduced F-termination while improving the stability and electrochemical performance of MXene [44]. The particular significance is the groundbreaking progress in acidic molten salt etching approach [45]. This method demonstrates excellent safety and efficiency. Niu *et al.* designed a layered porous MXene composite architecture, in which $Ti_3C_2$ nanosheets are alternately arranged with orthogonal $TiO_2$ nanoplates [46]. Obviously, the development of MXene synthesis strategies has received significant progress in three aspects, including minimizing environmental impact, improving operational safety, and achieving synthesis efficiency [47]. In addition, both CVD and PVD methods are typical "bottom-up" synthesis approaches [48]. Among them, CVD has become the main technology for fabricating high-quality MXene composite films [49]. Xu *et al.* [50] synthesized large-area and high-quality 2D ultrathin α-$Mo_2C$ crystals via CVD using molybdenum foil and $CH_4$ as precursors. The as-prepared α-$Mo_2C$ crystals exhibited a remarkably thin thickness of merely a few nanometers while maintaining lateral dimensions exceeding 100 μm. Moreover, Wang *et al.* [51] achieved *in situ* growth of MXene crystals on titanium substrates through thermal decomposition of a mixture of $CH_4$ and titanium tetrachloride gases at a high temperature of 950 °C. However, the strict requirements of CVD greatly increase process complexity and production costs including high-vacuum conditions and high temperatures. The LiF/HCl mixed etching system is currently the most widely adopted method, offering

advantages such as mild reaction conditions and minimal byproducts [52]. The resulting MXene nanosheets retain relatively abundant –O and –OH functional groups on their surfaces. In contrast, the emerging molten salt etching method enables the synthesis of MXene with higher crystalline quality under anhydrous conditions [53]. However, the resulting surface functional groups are relatively limited in variety, leading to reduced bonding affinity with the hydroxyl groups of cellulose [54].

**2.1 Solution mixing**

The solution mixing method has become a key method for fabricating MXene/nanocellulose composites, owing to its tunability in precisely controlling the integration of constituent materials within dispersed systems [55]. This complex approach can adjust the composition parameters and microstructure characteristics of the as-obtained composites [56]. MXene nanosheets mainly contribute to conductivity, while CNF dominates mechanical properties [57]. This method can construct complex structure such as 1D/2D interpenetrating networks, significantly enhancing electromagnetic wave absorption efficiency through optimizing impedance matching and dielectric loss characteristics [58]. For example, MXene/nanocellulose composites have achieved simultaneous improvement in mechanical strength, toughness, and EMI shielding performance via ammonium polyphosphate-assisted crosslinking [59]. The solution mixing method has applications potential in electromagnetic shielding systems and flexible electronic devices.

**2.2 Vacuum filtration**

The vacuum filtration method is the most commonly used fabrication method for the synthesis of MXene/nanocellulose composites due to its inherent simplicity and ease of operation [37]. During this process, the directional force caused by vacuum pressure facilitates effective material

assembly and endows the resulting composite with unique surface morphology. For example, Yang *et al.* [60] developed a sustainable GO/nanocellulose electromagnetic shielding composite film by *in-situ* mechanical exfoliation of graphite using vacuum filtration method, achieving an electromagnetic SE of 30.7 dB and an electrical conductivity of 3,172 S $m^{-1}$ at a minimal thickness of 40 μm (**Figure 2(a)**). Cao *et al.* [33] fabricated a MXene/CNF composite paper with a unique nacre-inspired "brick and mortar" microstructure through vacuum-assisted filtration (**Figure 2(b)**). At the beginning of tensile deformation, the extensive hydrogen bonding network between CNF and MXene nanosheets breaks. As the strain increases, relative sliding occurs between MXene nanosheets. CNF provides additional frictional energy dissipation between adjacent MXene nanosheets, effectively reducing sliding effects. Zhou *et al.* [61] synthesized an asymmetric sandwich-structured thin composite film via vacuum-assisted filtration, using CNF as the outer layers and MXene/AgNWs as the core interlayer (**Figure 2(c)**). The sandwich architecture maintains its structural integrity through a double-layer CNF, while the conductive core layer establishes a highly interconnected network. Although vacuum filtration offers operational simplicity, some inherent limitations constrain its industrial scalability [62]. The limited size of the filtering device directly determines the maximum achievable size of the composite. Two step vacuum filtration is a technical method that improves separation efficiency and selectivity through a staged filtration strategy. More recently, Lu *et al.* [63] developed a composite film with a conductive electromagnetic dual gradient structure. The composite film was prepared from CNF, MXene, AgNWs, and $Fe_3O_4$ by two-step vacuum filtration. In addition, liquid nitrogen-assisted vacuum filtration was developed to prepare composites by combining low-temperature technology with traditional vacuum filtration. Chang *et al.* [64] introduced ultrafine $RuO_2$ nanoparticles *in situ*

on highly conductive GeP nanosheets by liquid nitrogen-assisted liquid phase exfoliation and constructed $GeP_5$@$RuO_2$ nanocomposites with 0D/2D heterostructures. Furthermore, the filtration process often produces composites with high porosity, making them susceptible to the influence of moisture infiltration, leading to expansion and degradation in humid environments. Vacuum-assisted filtration method also has some disadvantages, such as high cost, high energy consumption, which is not suitable for large-scale production.

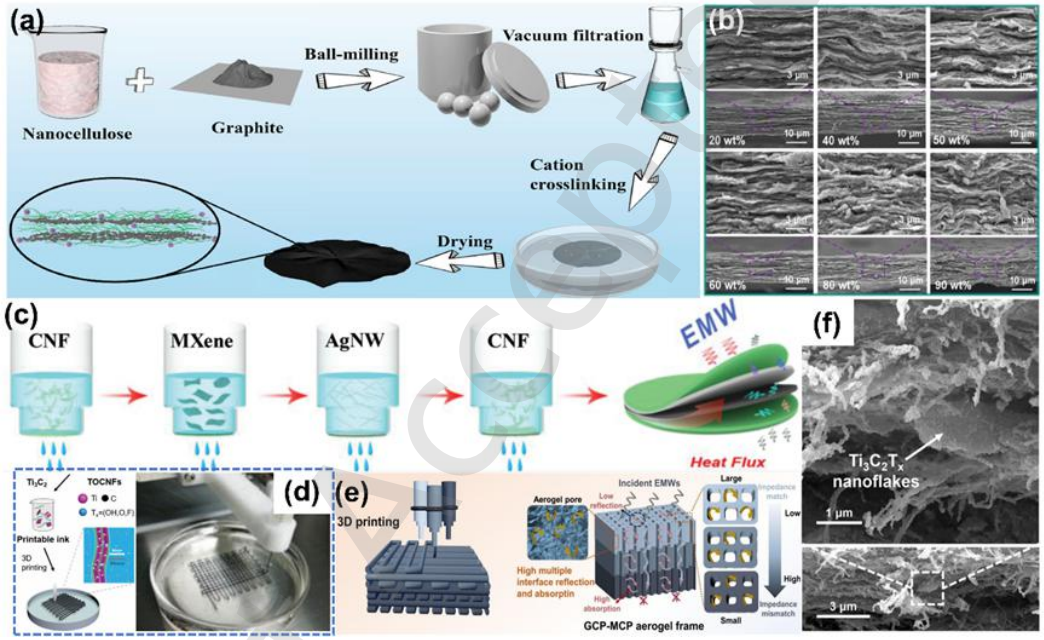


**Figure 2** The preparation strategies of MXene/nanocellulose composites. (a) Processing procedures of the cation crosslinking GO/nanocellulose composite films. Reproduced with permission from Ref. [60], © Elsevier 2023. (b) SEM images of the d-$Ti_3C_2T_x$/CNF composite paper, exhibiting a nacre-like compact lamellar structure. The weight content of d-$Ti_3C_2T_x$ in the d-$Ti_3C_2T_x$/CNF composite paper varies from 20 to 90 wt%. Reproduced with permission from Ref. [33], © American Chemical Society 2018. (c) Schematic of the LBL assembly of the CNF@MXene@AgNW composite film. Reproduced with permission from Ref. [61], © The Royal Society of Chemistry 2021. (d) Schematic illustration and optical images of TOCNFs/$Ti_3C_2$ fabrics. Reproduced with permission from Ref. [65], © Wiley-VCH GmbH 2020. (e) EMI schematic illustration of gradient structure with low reflection of the MS/CNF/PEDOT:PSS aerogel. Reproduced with permission from Ref. [66], © Elsevier 2025. (f) SEM images of PPy@BC/MXene composite film. Reproduced with permission from Ref. [67], © Springer Nature 2021.

### 2.3 3D printing

3D printing, as an advanced processing technology, enables the production of various flexible MXene/nanocellulose composites [68]. This technology helps solidify pre formed ink materials to construct 3D objects with complex geometric structures. By appropriately controlling the size and surface chemical properties of coordinated nanocellulose, the rheological and shear thinning properties of MXene based inks can be optimized even under low MXene loading. Cao *et al.* [65] pioneered the fabrication of macroscopic fibers through 3D printing of MXene/CNF hybrid inks, achieving precise assembly of 2D MXene nanosheets into flexible smart fibers with exceptional sensing properties for advanced textile applications (**Figure 2(d)**). From morphological perspective, the lamellar heterostructure represents typical configuration for achieving electromagnetic shielding and absorption [69]. The hydrogen bonding network established between the hydroxyl groups of cellulose and the surface functional groups of MXene not only facilitates load transfer but also enhances interfacial polarization [70]. Moreover, Chen *et al.* [66] fabricated a graded conductive porous MXene/CNF/poly(3,4-ethylenedioxythiophene):poly(styrenesulfonate) aerogel framework via direct ink writing 3D printing technology. Through the structural control from impedance matching to impedance mismatch, combined with the rich aerogel micropores in the top-down cis gradient configuration, the aerogel framework demonstrated an EMI SE of 106.43 dB (**Figure 2(e)**). The gradient structure is typically designed with stepwise variation in electrical conductivity from the incident surface to the transmission surface [71]. The incident layer, the intermediate transition layer, and the highly conductive layer collectively shift the shielding mechanism from surface reflection toward cyclic dissipation process of "absorption-reflection-reabsorption." The

gradient interface eliminates abrupt changes in properties between layers, endowing the material with combination of light weight, flexibility, and resistance to deformation, thereby avoiding the mechanically fragile nature inherent to purely porous structures.

### 2.4 Other methods

**Freeze-drying.** The freeze-drying method has used for fabricating MXene/cellulose composite aerogels and foams, owing to its cost-effectiveness and operational safety in the sublimation-based dehydration process [72]. It utilizes the abundant oxygen and hydrogen elements inherent in MXene and CNF, which helps to form a broad hydrogen bonding network during the freeze-drying process, effectively integrating MXene sheets into a robust macroscopic structure [73]. The as-obtained aerogels exhibit excellent properties, including ultra-high porosity, extremely low density, and excellent elasticity. Through precise control of ice template freeze-drying, anisotropic porous structures can be generated, thereby achieving customized mechanical properties along specific directions [74]. The abundant chemical active groups on the nanocellulose skeleton make it a promising material for high-performance composites. MXene/BC composites with different MXene contents can be prepared by chemical crosslinking between numerous -OH groups on nanocellulose chains or between -OH groups on cellulose chains and MXene (**Figure 2(f)**) [67].

***In-situ* biosynthesis.** The *in-situ* biosynthetic strategy plays a pivotal role in the development of MXene/nanocellulose composites [75]. A layered and densely arranged nanofiber structure with abundant electrochemical active sites was constructed by interweaving MXene layers of nanofibers. This composite is derived from the ternary layered MAX precursor of MXene and has

surface functional groups that are highly suitable for modification and active material loading. It reported that a thin PDA coating deposited on MXene substrates is an effective platform for *in-situ* generation of AgNPs, resulting in excellent thermal conductivity (**Figure 3(a)**) [76]. *In-situ* biosynthesis is a promising strategy for controlling the growth of cellulose nanoparticles on MXene surfaces, allowing for precise customization of composite structures [77]. This method ensures a strong interface contact between MXene and nanoparticles, thereby improving the overall performance of the resulting composite.

**LBL assembly**. The LBL assembly method has been widely investigated as a promising approach for constructing MXene/nanocellulose composites, which can precisely control the properties and structure of the composites [78]. The number of assembly cycles is directly related to the mass per unit area of the as-fabricated textile. Shang *et al.* [79] reported the synthesis of sandwiched CNF/boron nitride nanosheet/MXene composite films (**Figure 3(b)**). This multilayered architecture enables precise LBL assembly of composite, demonstrating remarkable EMI shielding capabilities. The MXene layers within composite film play a crucial role in electromagnetic wave reflection and absorption due to their unique properties. Furthermore, the layered structure amplifies electromagnetic wave interactions, thereby enhancing thermal energy dissipation [80]. The LBL assembly technique has been proven to be versatile and effective strategy for fabricating MXene/nanocellulose composites. This method shows considerable potential in achieving MXene/nanocellulose composites with excellent EMI shielding performance.

**Electrospinning**. CNF is as an environmentally friendly material with excellent mechanical properties, which can be used to construct MXene/CNF composites through spinning

technology [81]. In wet spinning, uniformly mixed composite dispersions are extruded into the coagulation bath through fine nozzles, while coaxial spinning provides significant flexibility in producing adjustable core-shell structured composite fibers [82]. Liu *et al.* [83] employed the technique to fabricate MXene-based core-shell fibers with strong mechanical strength and excellent conductivity, using GO/MXene as the conductive component and regenerated cellulose as the toughening matrix (**Figure 3(c)**). The resulting fibers typically exhibit high structural integrity and strong interfacial bonding. It is worth noting that MXene/nanocellulose composite fibers can be further woven into textiles, demonstrating great potential for flexible electronic devices. While all these strategies effectively integrate the two components, they exhibit marked differences in structural controllability, shielding mechanism, and scalability. Vacuum-assisted filtration yields dense architecture that predominantly reflects incident electromagnetic waves, incurring high risk of secondary pollution, and lacks internal porosity to exploit multiple reflection and scattering losses. Freeze-drying, by contrast, generates aligned channels or cellular structures that prolong the electromagnetic wave propagation path, significantly enhancing internal scattering and multiple reflections. Comparatively more refined technique, 3D printing enables the construction of millimeter- to centimeter-thick shielding bodies, rendering it well-suited for components of irregular geometries.

Regardless of the method employed, the insertion of cellulose nanofibers as structural scaffold between MXene interlayers readily gives rise to lamellar "brick-and-mortar" heterostructure [84]. In this architecture, the highly conductive MXene layers serve as "bricks" responsible for electromagnetic wave reflection and absorption, whereas the insulating cellulose layers function as "mortar" that tailors the interlayer spacing and optimizes impedance matching [85]. Owing to the

high aspect ratio and outstanding mechanical properties, cellulose nanofibers can impede crack propagation through "bridging" and "pull-out" mechanisms, thereby compensating for the inherent brittleness of MXene-based lamellar materials [86]. In general, high MXene content endows the composite with elevated electrical conductivity and superior shielding effectiveness, albeit at the expense of restricted interlayer sliding [87]. Conversely, high nanofiber cellulose content directly enhances the flexibility and fracture strain of the composite, yet the resulting sparse conductive network leads to considerable degradation in shielding effectiveness.

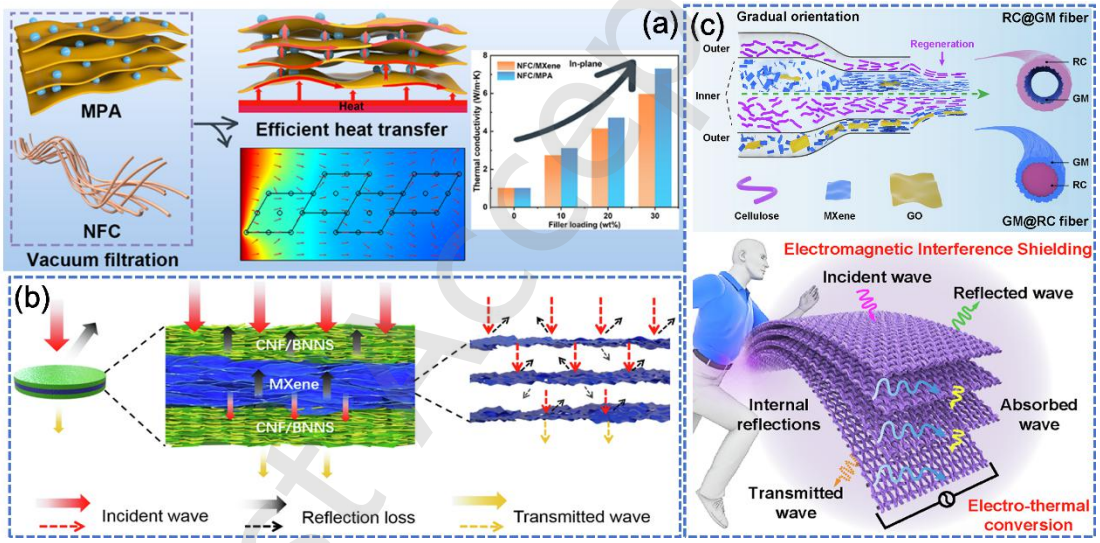


**Figure 3** Schematic illustration of the preparation, multifunctional applications of MXene-based composites. (a) Preparation and thermal conductivity of MXene/PDA/AgNPs composite film. Reproduced with permission from Ref [76], © Elsevier 2023. (b) Diagram of electromagnetic shielding mechanism of multilayer composite films. Reproduced with permission from Ref. [79], © Elsevier 2021. (c) Schematic illustration of solid GO/MXene@regenerated cellulose fiber and the resultant textiles of EMI shielding, solar-thermal and electro-thermal energy conversion applications. Reproduced with permission from Ref. [83], © Elsevier 2022.

### 3 Toughening mechanism of MXene/nanocellulose composites

In electromagnetic shielding applications, robust mechanical properties are crucial to ensure long-term performance and reliability. High strength, flexibility, and durability enable shielding

materials to withstand mechanical stress, vibrations, and environmental factors without damage [88-92]. For instance, flexible and lightweight shielding composites must maintain structural integrity under repeated bending or stretching, especially in wearable electronics or aerospace applications. Additionally, superior toughness can prevent cracking or delamination, which may affect the shielding effect [93,94]. Therefore, optimizing mechanical performance is crucial for developing high-performance and durable electromagnetic shielding solutions. In addition to the intrinsic hydrogen bonds between nanocellulose and MXene, the mechanical properties of MXene/nanocellulose composites can be further enhanced through physical strategies [95], chemical approaches [96], or their synergistic combination [97]. In this section, we reviewed the toughening mechanisms of MXene/nanocellulose composites based on physical toughening, chemical toughening, and synergistic toughening.

**3.1 Physical toughening**

The mechanical properties of MXenes, such as tensile strength and flexibility, are often limited by their inherent structural defects, weak interlayer van der Waals forces, and oxidation sensitivity [6,98]. Given the widespread application of EMI shielding materials in aerospace, wearable electronics, and telecommunications, where strong mechanical properties are crucial, pure MXenes often cannot meet practical requirements [99-103]. Nanocellulose's structure combines crystalline and amorphous regions, giving it excellent mechanical properties, including larger specific surface area, higher crystallinity (70%-80%), good Young's modulus, and easily adjustable physical and chemical properties [11,104-111]. The hydroxyl (−OH) groups of nanocellulose form hydrogen bonds with MXene surface terminations (=O, −F, −OH), improving interfacial adhesion [112]. In addition, the high-strength fiber network of nanocellulose serves as a

reinforcing scaffold, dispersing stress and preventing the re-accumulation of MXene layers. This hybrid structure reduces the brittleness of MXene while maintaining conductivity, thus forming a flexible and robust composite material with excellent mechanical properties [113]. Cao *et al.* [65] developed to prepare MXene/TOCNFs smart fibers and textiles (**Figure 4(a)**). The appropriate introduction of MXene nanosheets resulted in an obvious enhancement of the mechanical performance of the resultant composite fibers, compared with the pure TOCNFs (**Figures 4(b, c)**). The composite fiber with 30% MXene content demonstrated an optimal tensile strength of 136.5 MPa at 5% strain and high electrical conductivity (**Figures 4(d, e)**). As well as, Wan *et al.* [114] reported the preparation of ultra-thin, robust, and highly flexible $Ti_3C_2T_x$ MXene/BC composite films by *in-situ* biosynthesis method, in which MXene suspension was added to the culture medium of BC (**Figure 4(f)**). The composite film exhibits excellent mechanical properties, with a tensile strength of 297.5 MPa under a load of 25.7 wt% $Ti_3C_2T_x$, while maintaining a high EMI SE. In addition, the Young's modulus of $Ti_3C_2T_x$/BC composite film is higher than that of pure $Ti_3C_2T_x$ and pure BC (**Figures 4(g, h)**). Therefore, the appropriate addition of nanocellulose has a significant impact on the mechanical properties of MXene/nanocellulose composites.

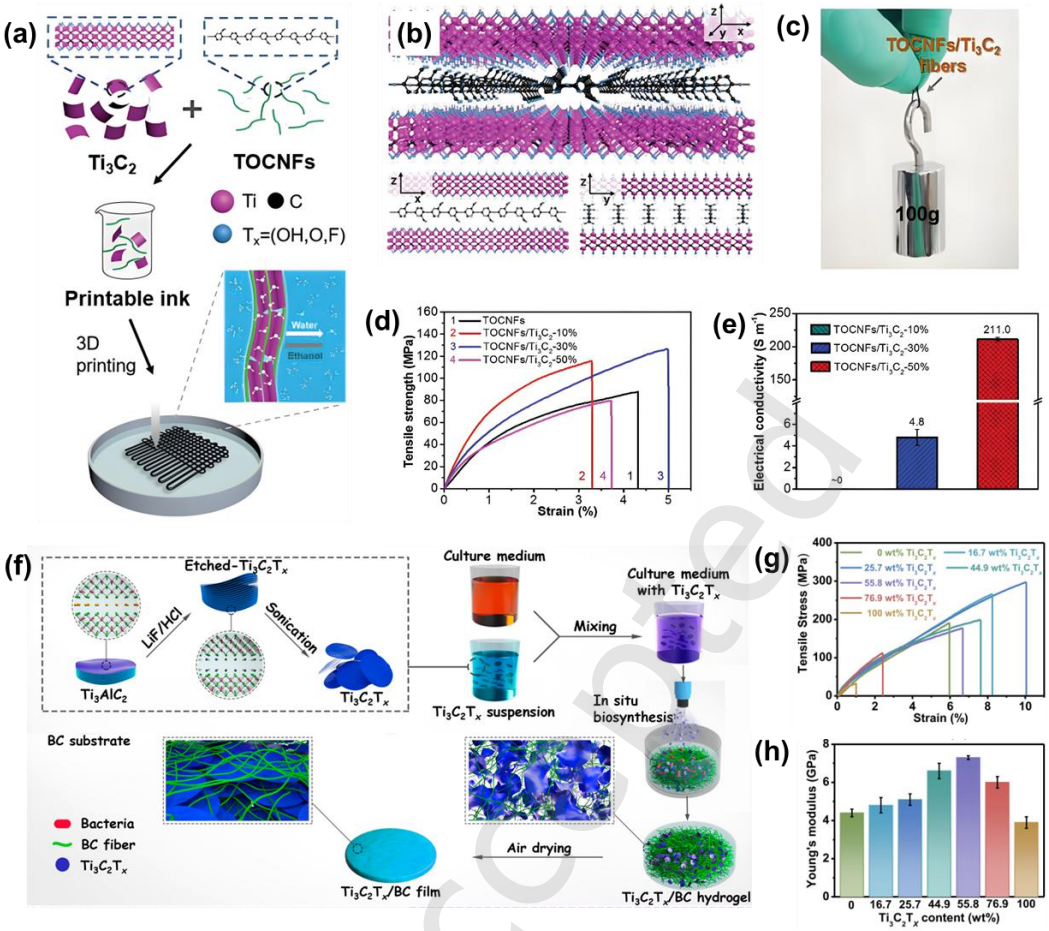


**Figure 4** The intrinsic hydrogen bond interactions and great mechanical properties of MXene/nanocellulose composites. (a) Schematic of the fabrication of the MXene/TOCNFs smart fibres and textiles. (b) Mechanism diagram of hydrogen bond interactions between MXene and TOCNFs; (c) Image of composite fibers holding 100 g weight; (d) Stress–strain curves, and (e) electrical conductivity of MXene/TOCNFs fibres. Reproduced with permission from Ref. [65], © Wiley-VCH Verlag GmbH 2019. (f) The fabrication process of MXene/BC composite films. (g) Stress–strain curves, and (h) Young's modulus of MXene/BC composite films. Reproduced with permission from Ref. [114], © American Chemical Society 2021.

In addition to the inherent hydrogen bonding interactions between nanocellulose and MXene, researchers have also developed various physical toughening strategies to further improve the mechanical properties of their composites. These methods mainly focus on three key mechanisms: (1) introducing additional hydrogen bonds and physically entangled networks, (2) implementing metal cation mediated ion crosslinking, and (3) constructing a reasonable architecture [115,116]. Each strategy employs different but complementary physical interactions to enhance the toughness

of materials while maintaining other ideal properties. The following section will discuss in detail these three basic toughening methods.

In order to improve the mechanical properties of composites, additional materials containing polar groups (such as sodium alginate, polyvinyl alcohol, etc.) can be added to the MXene/nanocellulose system [117,118]. These materials can introduce more hydrogen bonding sites, enhance electrostatic interactions, and promote physical entanglement between MXene, nanocellulose, and additives. Therefore, a denser hydrogen bonding network can be formed, further improving the overall mechanical properties of the composite [95,119]. A tough organic hydrogel with triple network structure was prepared from PVA, SA, and CNF (**Figure 5(a)**) [120]. GO is used to functionalize MXene nanosheets to form stable and uniform nanocomposites, which are then mixed into organic hydrogel matrix as conductive fillers. After adding SA and CNF, the tensile properties of the hydrogel were improved due to the hydrogen bond interaction between SA, CNF, and PVA molecular chains (**Figure 5(b)**). Furthermore, by adding MXene/GO nanocomposites, the as-obtained composite hydrogels reached the optimal breaking strain and tensile strength of 611.5% and 212.7 kPa, respectively (**Figure 5(c)**).

Researchers have also achieved excellent mechanical properties by constructing special structural systems for MXene/nanocellulose composites. Building a customized architecture (for example, aligned bionic porous gas gel or multi-layer vacuum filter composite film) in MXene/nanocellulose composites can improve their mechanical properties [16,121-124]. For example, the Zeng's team used the bidirectional freeze-drying method to assemble MXene/CNF aerogels with parallel micro pores [125]. The aerogels showed excellent mechanical strength and flexibility, and the compression modulus under 80% strain was as high as 280 kPa (**Figures**

**5(d,e)**). It can be inferred that the construction of this bionic arrangement porous structure mainly enhances the stress distribution, thus improving the compression modulus and compression resistance of the aerogel, while maintaining high EMI SE. In addition, CNF modified MXene (CM9) and CNC were combined into ANF network and Ag NW framework through multi-stage vacuum filtration, achieving super strong, super flexible, and conductive nano paper with layered structure [126]. In this graded nanoscale paper, CM9 forms a simulated "brick and mortar" microstructure of mother of pearl with ANF and Ag NW, significantly improving the mechanical properties of the composite. The obtained nano paper has excellent tensile strength (701.82 MPa), which is significantly better than the CNF/MXene composite film without multilayer structure mentioned above (341 MPa).

The ion crosslinking strategy enhanced the mechanical properties of MXene/nanocellulose composites by forming strong interfacial bonds between negatively charged MXene sheets and nanocellulose fibers via multivalent cations (e.g., $Ca^{2+}$, $Al^{3+}$, $Fe^{3+}$) [127,128]. These cations connect the oxygen-containing groups (-O, -OH) of the two components to form a robust 3D network. These ions act as crosslinking agents, forming ionic bonds and enhancing structural integrity [115,129,130]. Si's research team explored a proton exchange composite film design strategy based on a calcium ion-crosslinked CNF/SA composite network anchoring 2D MXene nanosheets (**Figure 5(f)**) [131]. In the CNF/SA composite matrix, $Ca^{2+}$ coordinated with carboxyl groups from both components, transforming the heterogeneous polymer chains from an amorphous state into a crosslinked and interlocked structure (**Figure 5(g)**). Meanwhile, MXene nanosheets with abundant hydrogen-bonding networks are firmly immobilized within the polymer network. As a result, the as-obtained CNF/SA/MXene composite film exhibited exceptional

mechanical strength and stability (164.7 MPa) (**Figure 5(h)**).

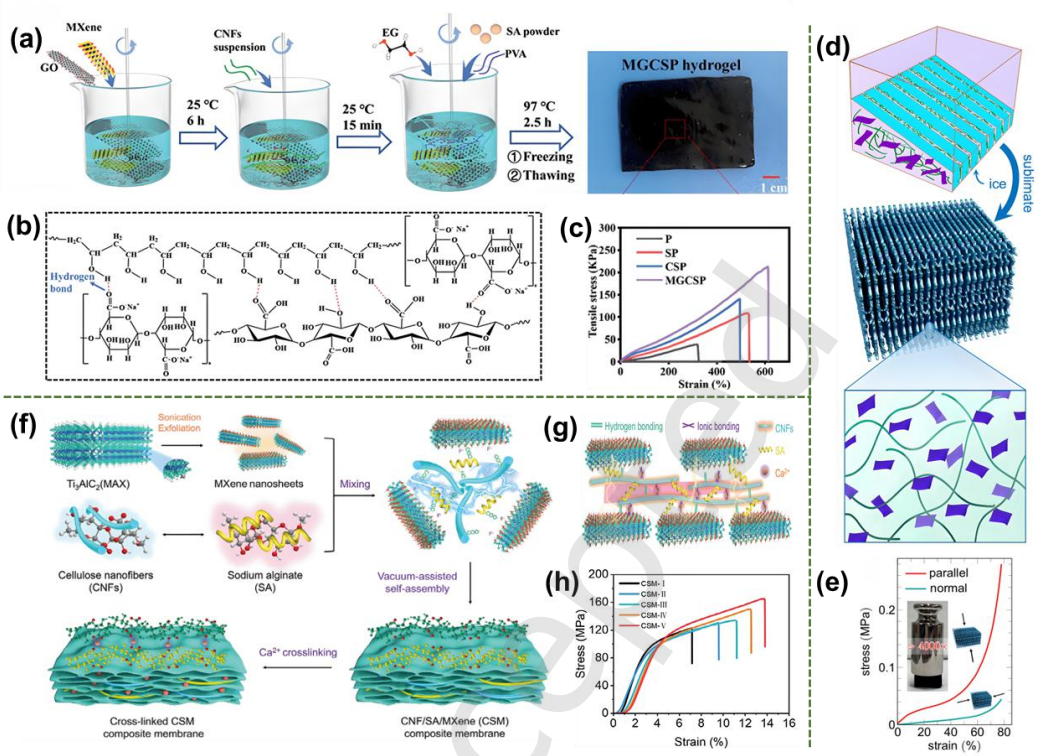


**Figure 5** The physical toughening methods for MXene/nanocellulose composites. (a) Schematic diagram of the preparation process of MGCSP hydrogel. (b) Illustration of hydrogen bonding and physical entanglement between materials. (c) Stress–strain curves of MGCSP hydrogel. Reproduced with permission from Ref. [120], © Royal Society of Chemistry 2022. (d) Schematic illustration for the fabrication of MXene/CNFs hybrid aerogels with oriented biomimetic cell walls. (e) Compression curves of MXene/CNFs aerogels. Reproduced with permission from Ref. [125], © American Chemical Society 2021. (f) Schematic illustration of the synthesis of CNFs/SA/MXene composite film based on a calcium ion-crosslinking. (g) Schematic illustration of the ionic and hydrogen bonding network formed among $Ca^{2+}$, SA, CNFs, and MXene. (h) The stress-strain curves of cross-linked CNFs/SA/MXene composite films. Reproduced with permission from Ref. [131], © Wiley-VCH Verlag GmbH 2025.

### 3.2 Chemical toughening

The fundamental distinction between physical and chemical toughening in MXene/nanocellulose composites lies in their bonding mechanisms. Chemical toughening establishes permanent covalent networks through surface modifications like silane coupling (forming Si−O−C/Ti bonds) and PDA coating (creating catechol crosslinks), resulting in irreversible, high-strength interfaces.

These covalent bonds provide excellent mechanical stability and load transfer capabilities [132-134]. Conversely, physical toughening employs reversible interactions: hydrogen bonding between hydroxyl groups, physical entanglement of nanofibers, structure construction, and ionic crosslinks via metal cations [135]. Chemical toughening yields superior mechanical properties through stable covalent bonding, physical methods offer dynamic adaptability and energy dissipation via breakable/reformable bonds [136]. The covalent networks in chemical toughening enhance modulus and fracture resistance significantly, whereas physical interactions enable self-healing and flexibility. The selection of toughening strategies depends on specific application requirements, where chemical toughening enhances structural integrity while physical toughening improve adaptability and dynamic performance [137].

Given the intrinsic hydrogen-bonded physical crosslinking in MXene/nanocellulose composites, the term chemical toughening strategies herein denotes chemical crosslinking or modification methods implemented to augment this inherent physical network. The chemical toughening strategy primarily involves two approaches: (1) chemical modification of MXene and nanocellulose themselves to enhance interfacial interactions between the two materials [138], and (2) chemical treatment of the MXene/nanocellulose composites (e.g., through silanization, polyurethane modification, or PDA coating) to establish robust covalent networks [139]. These approaches significantly improve mechanical properties and enhance structural stability. By first quaternized CNF (QACNF) and then integrating it with MXene nanosheets into a covalent polymer network, Li *et al.* [140] developed a hydrogel exhibiting unprecedented mechanical balance with 449 kPa tensile strength, 1700% elongation, and 5.46 MJ/m$^3$ toughness, outperforming conventional formulations. The quaternization modification of CNF introduces

quaternary ammonium groups that can form electrostatic interactions with oxygen-containing groups on MXene surfaces, resulting in a bridging effect that facilitates the interlinkage among adjacent MXene nanosheets. It guarantees the construction of connecting and reliable conductive network. Also, the use of silicone crosslinker with multi-functional groups, and hyperbranched polysiloxane, can boost the formation of covalent bonds, thus guaranteeing the high mechanics of backbone structure. Furthermore, Sun's research team prepared a composite film composed of PDA-modified MXene/BC through an *in-situ* spontaneous oxidative polymerization and vacuum-assisted filtration process (**Figure 6(a)**) [139]. Dopamine was oxidized into dopamine quinone under the action of dissolved oxygen, followed by a series of cyclization, oxidation, and isomerization processes. Eventually, through self-polymerization and coordination polymerization, a thin PDA monolayer formed on the surface of MXene (**Figure 6(b)**). BC was embedded into the PDA-modified MXene nanosheets and interconnected via hydrogen bonds, forming a compact layered structure. This endowed the composite film with excellent tensile strength (406 MPa) and toughness (15.3 MJ $m^{-3}$) (**Figure 6(c)**). Above chemical toughening of chemically modifying nanocellulose or MXene themselves to enhance the mechanical properties of composites primarily involves introducing functional groups through modification to strengthen interactions between materials. Alternatively, the modification enables covalent bonding, which improves the inherent strength while promoting stronger interactions with the other material in the composites.

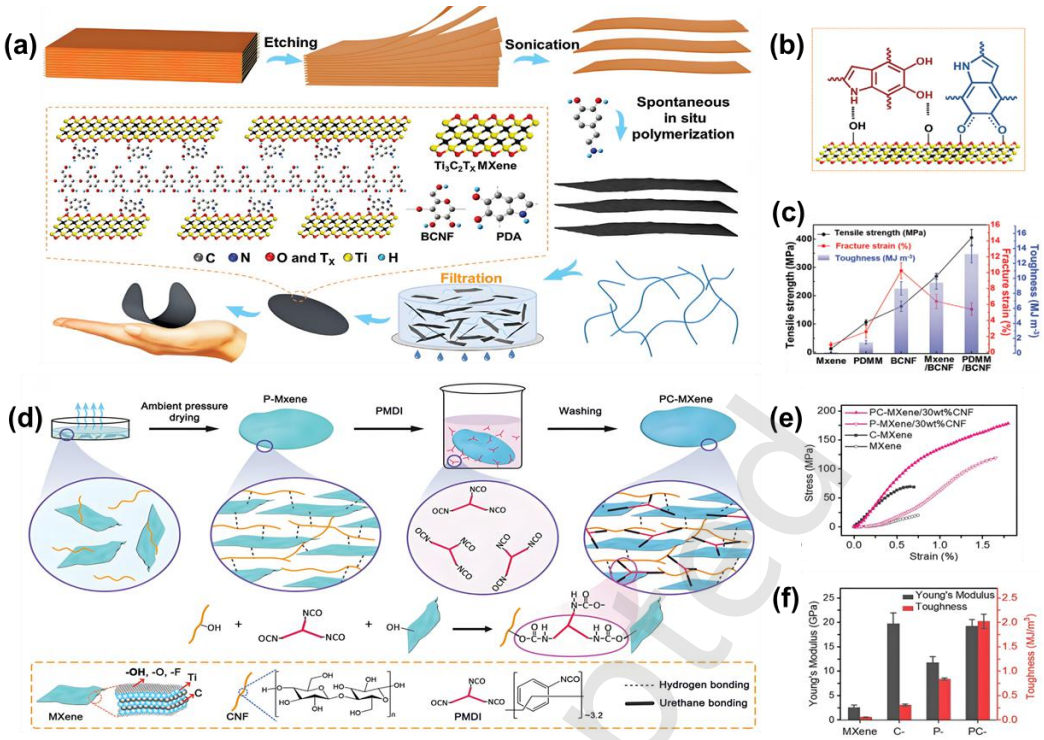


**Figure 6** The chemical toughening methods for MXene/nanocellulose composites. (a) Preparation flowchart of PDA covalently crosslinked modified MXene/BC composite film. (b) Proposed binding mechanism of PDA to MXene. (c) Tensile strength and toughness. Reproduced with permission from Ref. [139], © Wiley-VCH Verlag GmbH 2021. (d) Schematic illustrating the fabrication process of PMDI-chemically crosslinked MXene/CNF composite film. (e) Tensile stress–strain curves. (f) Modulus and toughness. Reproduced with permission from Ref. [96], © Wiley-Blackwell 2021.

Relatively few studies have been focused on improving mechanical properties through chemical modification of MXene and nanocellulose themselves. Instead, most research has concentrated on further chemical modification of MXene/nanocellulose composites [141]. Gustav Nyström *et al.* fabricated MXene/CNF composite films via ambient-pressure drying, followed by chemical crosslinking treatment with PMDI (**Figure 6(d)**) [96]. The PMDI reacts with both MXene and CNF to form a covalent crosslinked network, substantially enhancing the mechanical properties. The modified composite films demonstrated remarkable improvements in tensile strength (160 MPa), modulus, and mechanical toughness, representing 786%, 646%, and 3383% enhancements, respectively, compared with pristine MXene composite films (**Figures 6(e,f)**). Moreover, Tang's team reported a groundbreaking self-adhesive PDMS foam featuring a nanoscale worm-like structure with residual Si−H reactive groups, fabricated through a foaming process at room temperature via organosilicon chemical reactions [136]. This self-adhesive PDMS foam can be

directly decorated with a hybrid MXene/CNF interconnected network through multiple physicochemical interactions between the nanocoating and foam substrate. The resulting composites demonstrate remarkable mechanical flexibility (compressive stress of 90 kPa at 70% strain), with nearly unchanged stress values after 100 compression cycles. Besides, Pan *et al.* [142] proposed a universal pH-triggered strategy for modulating MXene spinning dopants by selecting carboxylated cellulose nanofibers (CNF-C) as additives. By adjusting the pH, multiscale sheet-wire linkages covalent bonds were controllably formed through nucleophilic substitution and dehydration reactions, thereby enhancing mechanical strength to construct high-performance MXene fibers. A substantial number of C−O−Ti covalent bonds formed within the MXene/CNF-C fibers, promoting the ordered alignment of MXene nanosheets during spinning and achieving a high tensile strength of 258 MPa. The key feature of chemical toughening lies in introducing crosslinkers or modifiers to chemically modify MXene/nanocellulose composites. Beyond the physical hydrogen-bonded network between nanocellulose and MXene, this approach establishes a robust covalent crosslinking network, further enhancing the mechanical strength of composites. Common chemical toughening agents (e.g., PDA, PDMS, etc.) improve mechanical performance and impart hydrophobic properties to the composites [143]. Compared with physical toughening, chemically modified composites exhibit superior structural stability. However, some modifiers (e.g., PDMS) are difficult to biodegrade, whereas physical toughening strategies offer advantages in terms of sustainability and recyclability. Besides, although covalent bonding and surface modification layers effectively enhance interfacial adhesion and toughness in chemically toughened EMI shielding composites, the long-term chemical stability and potential degradation behavior under extreme service conditions like sustained high temperature, high humidity, and prolonged stress fatigue remain critical yet underexplored aspects. Notably, while offering superior strength over physical adsorption, Si-O-C bonds are susceptible to hydrolytic back-reaction under prolonged high-temperature exposure, particularly in the presence of acidic or alkaline conditions [144,145]. Water molecules are highly polar species, readily penetrate interfacial micro-defects and reach covalent bonding regions. Si-O-Ti are prone to hydrolysis in a high-humidity environment, leading to progressive decoupling of chemical bonding. Furthermore, PDA exhibits intrinsic hydrophilicity, the non-covalent π-π stacking domains may absorb moisture

and swell under high humidity and generate internal stress that promotes interfacial cracking [146,147]. Therefore, the stability of the covalent network under extreme EMI shielding environments still needs to be further strengthened.

### 3.3 Synergistic toughening

Researchers increasingly favor synergistic physical-chemical toughening strategies for MXene/nanocellulose composites due to their complementary advantages [148]. The physical hydrogen-bond network enables energy dissipation and flexibility, while chemical crosslinking (e.g., C−O−Ti bonds) provides robust strength and stability. These dual approaches overcome the limitations of single method, achieving an optimal balance between high strength, toughness, and functionality [149]. Moreover, it allows tunable interfacial interactions and multi-scale structural control, making it versatile for diverse applications. The sacrificial physical bonds (hydrogen bonds, ionic links) dissipate substantial energy through reversible breaking/reforming, delaying crack initiation [150]. At the same time, the persistent covalent network maintains cohesion, prevents crack propagation caused by physical bond breakage, and ensures high ultimate strength while enhancing toughness. Compared to using any single strategy alone, this combination can achieve excellent fracture resistance.

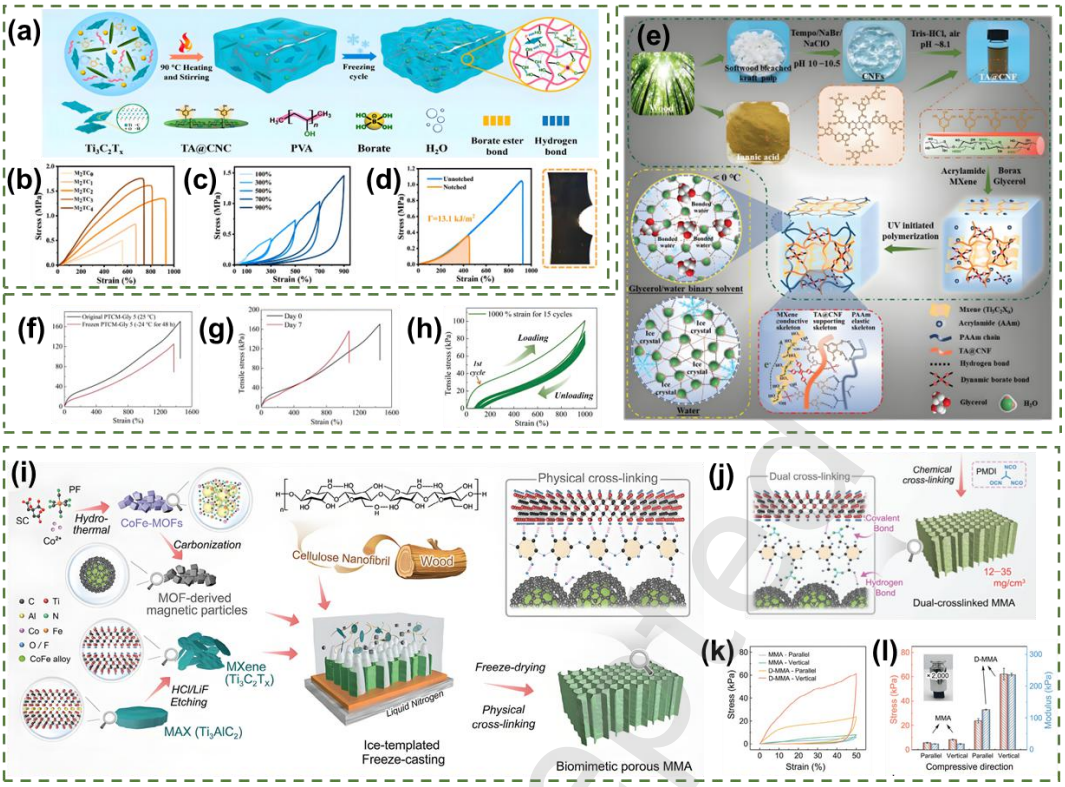


**Figure 7** Synergistic toughening strategies for MXene/nanocellulose composites. (a) Preparation process of functional hydrogels with synergistic hydrogen bonding and boronate ester networks. (b) Tensile stress–strain curves, (c) gradient strain cyclic loading–unloading tests, and (d) tensile stress–strain curves of both unnotched and notched hydrogels. Reproduced with permission from Ref. [151], © Elsevier 2025. (e) Preparation process of TA@CNF/PAAm/MXene hybrid hydrogels and schematics illustrating the hydrogen bonding and chemical bonding between the MXene, TA@CNF, and PAAm elastic networks. (f) Tensile stress–strain curves of frozen hybrid organ hydrogels. (g) Tensile stress–strain curves of organ hydrogels before and after exposing for 7 days. (h) Cyclic loading–unloading curves of organ hydrogels under a strain of 1000% for 15 cycles. Reproduced with permission from Ref. [152], © Wiley-VCH Verlag GmbH 2020. (i) Schematic showing the fabrication process of biomimetic ordered CNFs/MXene/MOF-derived CoFe@carbon aerogel. (j) Dual crosslinking mechanism. (k) Typical compressive stress–strain curves of aerogel with and without dual crosslinking in the directions of parallel and vertical to pore channels. (l) Maximum compressive stress and Young's modulus in the parallel and vertical directions. Reproduced with permission from Ref. [153], © Wiley-VCH Verlag GmbH 2024.

The researchers studied the double crosslinked network MXene/nanocellulose hydrogel based on dynamic hydrogen bond and covalent bond, and showed excellent tensile properties. For example, a multifunctional hydrogel was prepared by integrating MXene and tannic acid coated carboxylated cellulose nanocrystals (TA@CNC) Containing PVA and borax (**Figure 7(a)**) [151].

The synergistic effect of dynamic hydrogen bonds and dynamic borate ester bonds forms a dynamic 3D network, while the flexible covalent crosslinked network combined with the rigidity of TA@CNC endows the hydrogel with exceptional tensile strength, strain (1.35 MPa, 930%) and tear resistance (**Figures 7(b-d)**). Furthermore, the fabrication of conductive organ hydrogels was reported by incorporating MXene nanosheets into a tannic acid-modified CNF (TA@CNF)/polyacrylamide (PAAm) hybrid gel network (**Figure 7(e)**) [152]. This system features a ternary network structure combining a mechanically robust TA@CNF framework, a covalently crosslinked PAAm network, and a conductive MXene nanosheet network. The abundant presence of catechol groups along with dynamic reversible interactions, including hydrogen bonds and borate ester bonds, enables the hydrogel to achieve good fatigue resistance, environmental stability, and remarkable stretchability with strains reaching up to 1500% (**Figures 7f-h**). These findings demonstrate that constructing dual-network hydrogels through hydrogen bonds and covalent bonds in MXene/nanocellulose systems can effectively synergize to enhance the tensile properties of hydrogels.

To enhance the compressive performance and structural stability of MXene/nanocellulose aerogels, researchers typically employ a synergistic approach combining physical strategies (such as biomimetic pore structure construction) with chemical covalent crosslinking strategies. Qiao *et al.* [153] employed a dual crosslinking strategy combining physical and chemical approaches with CNFs as mediators to tightly integrate MXene and magnetic MOF-derived CoFe@carbon nanoparticles, constructing an ultralight yet robust magnetic MXene aerogel (**Figure 7(i)**). The aerogel, fabricated via typical ice-templated freeze-casting, exhibits a distinctive biomimetic honeycomb porous microstructure with cell walls aligned along the ice crystal growth direction.

The system features hydrogen-bonded physical crosslinking among CNFs, MXene, and magnetic MOF-derived CoFe@carbon nanoparticles. Subsequent chemical crosslinking with PMDI promoted covalent bond formation between components (**Figure 7(j)**). This dual-crosslinking approach remarkably enhanced the aerogel's mechanical robustness, demonstrating a compressive stress of 62.2 kPa at 50% strain. Compared to solely physically crosslinked MMAs (magnetic MXene aerogels), the compressive modulus increased by 706% in the parallel direction and 1311% in the vertical direction (**Figures 7(k, l)**). Moreover, the aerogel demonstrates exceptional electromagnetic wave absorption performance, achieving a maximum absorption intensity of −63.9 dB and a specific reflection loss of −1105 dB $mm^{-1}$. These values are comparable to the best MXene-based electromagnetic wave absorbers reported to date. In summary, the integration of nanocellulose/MXene composites with ice-templating freeze-drying technology has yielded preliminary advancements in scalable fabrication; nevertheless, the approach remains in the transitional phase from laboratory-scale research to pilot-scale production [154]. Through precise regulation of slurry concentration, freezing temperature, and annealing protocols, composites featuring oriented porous architectures can be achieved. However, the scalability of the method is constrained by the consistency of thermal gradients and crystallization behavior during the freezing process, rendering structural inhomogeneities inevitable in large-dimension samples [155]. Although this technique demonstrates considerable potential for scale-up in domains such as high-efficiency electromagnetic interference shielding, piezoresistive sensing, and energy storage electrodes, realizing industrially viable scalable manufacturing necessitates further breakthroughs in freeze-casting mold design, energy efficiency, and drying time optimization.

Also, Zeng's research team developed an ambient-pressure drying (APD) method for preparing CNF/MXene aerogels, incorporating PMDI as chemical crosslinking agent [156]. The combined effects of ethanol solvent exchange treatment, the APD approach, and hydrogen bonding interactions between CNF and MXene facilitated the formation of biomimetic cell-wall structures, thereby enhancing the aerogel's mechanical strength. Meanwhile, the aerogel demonstrates exceptional shielding performance of 64 dB at an ultralow density of 18 mg/cm$^3$. In summary, the synergistic toughening of MXene/nanocellulose aerogels requires careful consideration of pore structure effects. While incorporating additional materials and chemical modifications enhances compressive properties and structural stability, these strategies concurrently improve EMI shielding/absorption performance, leading to overall enhancement of the aerogel's comprehensive properties.

It is noteworthy that Cheng's team placed particular emphasis on composite film porosity and interfacial interactions, which constitute critical factors for enhancing stress transfer efficiency in MXene composite films [26]. They developed ultra-strong macroscopic MXene composite films by sequentially bridging MXene nanosheets with LM and BC (termed LBM composite films), achieving remarkable tensile strength of 908.4 MPa. The incorporation of LM and the LBL coating-based physical structure construction effectively reduce the voids within the thin composite film, while BC strengthened interfacial interactions between MXene nanosheets through hydrogen bonding and LM via coordination bonding (Ti-O→$Ga^{3+}$ and C-O→$Ga^{3+}$). Simultaneously, the LBM composite film with a thickness of 1.1 μm demonstrated an ultrahigh specific EMI SE of 23,600 dB·mm$^{-1}$. Furthermore, an effective densification strategy based on

sequential hydrogen and covalent bonding was explored for the fabrication of CMC/borate ion/MXene composite films by Cheng *et al.* [157]. While nanocellulose was not selected as the matrix, a similar synergistic toughening mechanism was adopted. The combined effects of CMC's filling/binding capability and borate ions' covalent bridging resulted in synergistic densification, endowing the composite film with enhanced mechanical properties, including a remarkable tensile strength of 583 MPa. From the perspective of composite film porosity and densification, the sequential bridging of hydrogen and covalent bonds, combined with strategically designed structural construction, can yield superior tensile strength compared to other reported studies. Obviously, whether for hydrogels, aerogels, or composite films, the synergistic toughening strategy combining physical approaches (hydrogen bonding and structural construction) and chemical methods (covalent bonding, etc.) can significantly enhance the mechanical properties of MXene/nanocellulose composites. The physical network provides reversible energy dissipation and toughness, while the chemical network supplies a framework for strength and stability. Hence the synergistic toughening synergy achieves a unique combination of high strength, high toughness, structural stability, and enhanced multifunctionality that neither approach can realize alone. Notably, controlling material porosity and densification degree proves crucial for mechanical reinforcement. Compared to individual physical or chemical toughening approaches, this synergistic strategy demonstrates superior comprehensive performance, including enhanced mechanical properties, improved stability, and excellent EMI shielding capability. More important, the mechanical properties of composite materials do not merely aim for high values. When designing electromagnetic shielding composites for specific applications, an appropriate mechanical grade should be selected according to the actual service conditions rather than

pursuing the highest strength due to the fact that cost considerations cannot be ignored.

### 3.4 Medium and structure effect on microwave absorption performance

In addition to mechanical properties, emerging mechanisms such as the medium effect offer new capabilities to modulate microwave absorption performance. Unlike traditional approaches that rely solely on composition or morphology control, the medium effect enables fine-tuning of dielectric and magnetic loss behavior at the microscopic level, to which electrostatic interactions contribute as one of the new methods. Specifically, electrostatic interactions at filler-matrix interfaces and within polar functional groups influence charge distribution, dipole orientation, and local electric fields, thereby affecting interfacial polarization and dipole relaxation processes that are critical for dielectric loss [158]. The medium plays a pivotal role in tuning the microwave absorption performance, as it governs the trade-off between impedance matching and attenuation capacity. These two requirements are essential yet often conflicting for achieving efficient absorption. A standalone microwave absorber typically possesses excessively high permittivity or permeability, leading to severe impedance mismatch with free space and thus predominant reflection of incident waves. Incorporating the absorber into a suitable medium enables the effective electromagnetic parameters to be adjusted toward the characteristic impedance of air, facilitating wave penetration [159]. Furthermore, the medium contributes additional dielectric loss mechanisms, including interfacial polarization at filler-matrix interfaces, dipole polarization from polar functional groups, and multiple reflections within porous architectures, while simultaneously suppressing undesirable effects such as eddy currents and filler aggregation [160]. The morphological configuration of MXene/cellulose composites plays an important role in determining both mechanical properties and microwave absorption performance [161]. In lamellar

structures, typically achieved through ice-templating or layer-by-layer assembly, alternating MXene and cellulose layers create abundant heterointerfaces that promote multiple reflections and interfacial polarization, significantly improving electromagnetic wave attenuation. Simultaneously, the aligned lamellar architecture facilitates efficient load transfer along the layer direction, enhancing tensile strength and toughness [162]. In porous structures, the introduction of interconnected voids reduces the effective permittivity, improving impedance matching with free space, while the cellular walls act as multiple scattering centers for incident waves. From a mechanical perspective, porous structures dissipate energy through cell wall buckling and densification under compression, offering enhanced toughness and deformation tolerance.

Rational design of the medium and structure is indispensable for translating the intrinsic loss capability of absorbents into practical high-performance microwave absorbers. Therefore, while pursuing enhanced mechanical properties such as strength and toughness, equal attention must be paid to the rational design of the medium to ensure that the intrinsic microwave absorption capability of the absorbents is not compromised but rather synergistically integrated [163,164]. The comprehensive data comparison of MXene/nanocellulose composites is displayed in **Table 1**.

**Table 1**. Comprehensive data comparison table of MXene/ nanocellulose composites.

| Composites | Preparation | Tensile/ strength | Strain | Modulus | EMI SE | Ref. |
|---|---|---|---|---|---|---|
| MXene/CNF/PMDI | Ambient pressure drying | 160 MPa | ~1.75% | - | 55.0 dB | [96] |
| $Fe_3O_4$/CNT/CNF/MXene | Vacuum filtration/hot-pressing | 119 MPa | ~4.5% | - | 49.1 dB | [165] |
| MXene/CNFs/CoNi | Vacuum filtration/lyophilization | 0.55 MPa | ~95% | - | 51.0 dB | [166] |
| GF/MX-CNF | vacuum | 89 MPa | ~5.2% | 1.58 GP | 43 dB | [167] |

| | | | | | | |
|---|---|---|---|---|---|---|
| composite films | filtration | | | a | | |
| J-MLCNF/TM | Vacuum filtration/hot-pressing | 72.69 MPa | - | - | 36.22 dB | [168] |
| CNFs/MXene hydrogel | Radical polymerization | 449 kPa | 1706% | 74 kPa | - | [140] |
| CNF/MXene/CNC | Vacuum filtration/hot-pressing | 701.82 MPa | ~23% | 12.98 GPa | 62.28 dB | [169] |
| TOCN/MXene | Vacuum filtration | 124.6 MPa | ~26% | - | 36 dB | [170] |
| MXene/TOCNFs | 3D printing | 136.5 MPa | 5% | 9.3 ± 2.4 GPa | - | [58] |
| CNF/MXene | Vacuum filtration | 532.87 MPa | 12% | 8.02 ± 0.64 GPa | 20 dB | [171] |
| CNF/MXene/ZIF-67 | Vacuum filtration | 12.8 MPa | 7% | - | 62.4 dB | [37] |
| LBM composite films | Blade coating | 908.4 MPa | 2% | ~17 GPa | 58.2 dB | [26] |
| MGCSP organo-hydrogel | Freezing-thawing | 212.7 kPa | 611.5% | ~25KPa | - | [120] |
| CNF/MXene Nanocomposites | Freezing-thawing | 280 kPa | 80% | - | - | [125] |
| CNF/SA/MXene | Vacuum filtration | 164.7 MPa | 14% | - | - | [131] |
| TA@CNC | Freezing-thawing | 1.35 MPa | 930% | - | - | [151] |
| $Ti_3C_2T_x$ MXene/BC composite films | *In-situ* biosynthesis method | 297.5 MPa | 10% | 5.1 GPa | - | [114] |
| MXene/CNF-C | Wet-spinning | 258 MPa | ~0.66% | - | - | [142] |
| PDMS/MXene/CNFs | Dip-coating | 90 kPa | 70% | - | - | [136] |
| PDMM/BCNF composite film | Vacuum filtration | 406 MPa | ~5.5% | - | - | [139] |

## 4 Structural designs of MXene/nanocellulose composites

The MXene nanosheets exhibit excellent hydrophilicity due to the presence of surface functional groups such as -F, -O, and –OH [172]. Nanocellulose, rich in oxygen-containing groups, can interact with other materials through various intermolecular forces. Consequently, the MXene/nanocellulose composite can be fabricated into diverse architectures including fibers, thin composite films, aerogels, and hydrogels. Through multidimensional structural design, precise regulation of electromagnetic wave attenuation mechanisms and material performance can be achieved, with the structural configurations primarily categorized into three main types: 1D fibrous structure, 2D layered assemblies, and 3D interconnected networks [93,173-175].

### 4.1 1D fiber structure

In MXene/nanocellulose composite systems, 1D fiber architectures typically refer to continuous fibers with ultrahigh aspect ratios (**Figure 8(a)**) [176]. The ordered alignment of fibrous macromolecules endows these composites with exceptional mechanical properties, including superior tensile strength, bending flexibility, and structural stability [177]. Furthermore, MXene/nanocellulose composites demonstrate remarkable characteristics, such as lightweight construction, environmental durability, conformal skin adhesion, and tunable elasticity, coupled with inherent biocompatibility [178]. These properties above make them ideal candidates for next-generation wearable EMI shielding devices, especially in applications requiring mechanical compliance and bio-interfacial compatibility (**Figure 8(b)**) [179].

**Electrostatic spinning fiber.** The electrostatic spinning method uses a high-voltage electric field to electrically charge a polymer solution or melt, forming a jet that is stretched and cured in the electric field to obtain nano or micron-sized fibers. Electrostatic spinning enables the

fabrication of continuous fibers with diameter control spanning from tens of nanometers to micrometers (**Figure 8(c)**) [180]. The controllable alignment of these fibers facilitates the formation of continuous conductive pathways, thereby enhancing bulk electrical conductivity. The intrinsic porous architecture within the fiber networks promotes multiscale electromagnetic wave scattering and absorption phenomena, significantly improving EMI shielding effectiveness. Pioneering work by Sobolciak *et al.* [181] established the electrospinning protocol for $Ti_3C_2T_x$ MXene/CNF-reinforced PVA nanofibers, achieving remarkable electrical conductivity (> 0.8 mS/cm) and elastic modulus (855 MPa). These breakthrough parameters demonstrate exceptional promise for flexible wearable EMI shielding applications, particularly in scenarios requiring simultaneous mechanical resilience and dynamic electromagnetic protection. The porosity of the fiber composite film from electrostatic spinning can reach 80%-95%, with excellent air permeability.

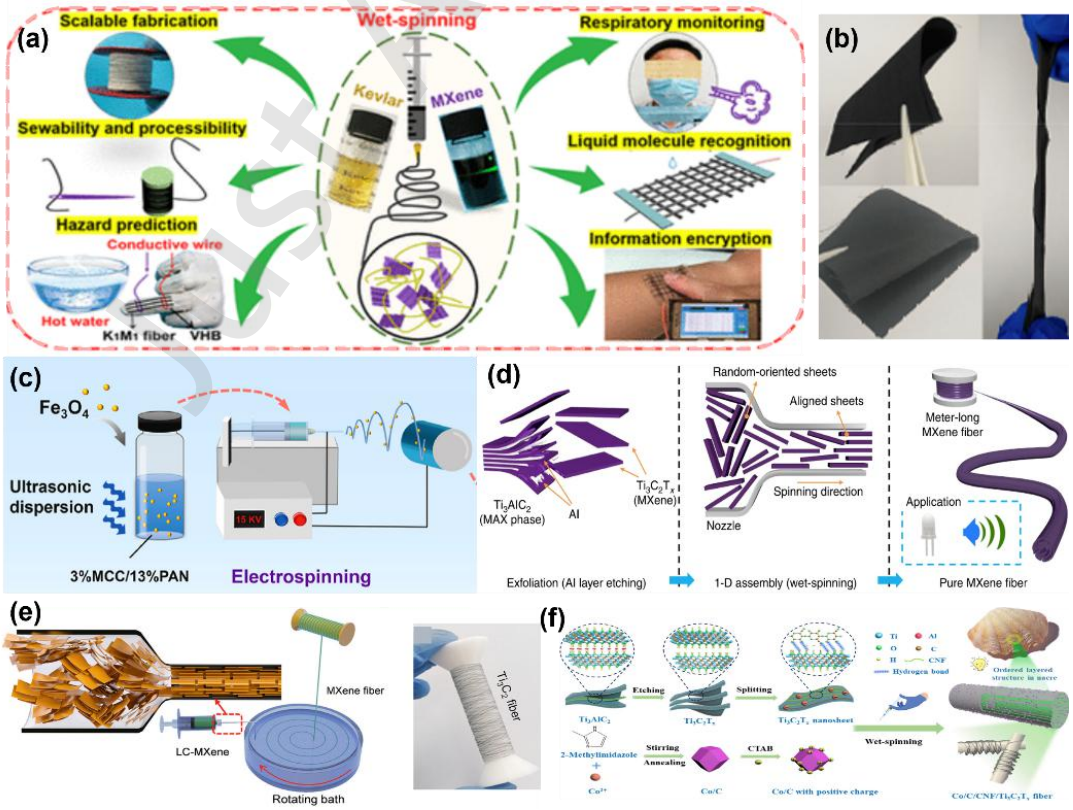

**Figure 8** Electromagnetic shielding composite materials with a 1D fiber structure. (a) Preparation of CNF/MXene fibres by wet spinning. Reproduced with permission from Ref. [176], © American Chemical Society 2021. (b) CNF/MXene fibres woven into fabrics. Reproduced with permission from Ref. [179], © American Chemical Society 2020. (c) Electrostatic spinning into fibrous fabrics. Reproduced with permission from Ref. [180], © Elsevier B.V. 2024. (d) Schematic diagram of the reconstruction of MXene into MXene fibres by wet spinning. Reproduced with permission from Ref. [182], © Zhang J. Z. et al. 2020. (e) Schematic diagram of the wet spinning process. Reproduced with permission from Ref. [183], ©American Chemical Society 2020. (f) Synthesis mechanism of Co/C/CNF/$Ti_3C_2T_x$ fiber. Reproduced with permission from Ref. [184], © Elsevier B.V. 2024.

**Wet spinning fiber.** Wet spinning, on the other hand, involves squeezing a polymer solution into a coagulation bath and solidifying it through phase separation to form fibers. Wet-spin fibers have better mechanical properties and may be more suitable for textiles or composites. Compared to electrospinning, wet spinning offers mature processing, broad applicability, superior fiber performance, and lower investment costs, making it a widely adopted method for preparing MXene/nanocellulose composites (**Figure 8(d)**) [182]. Uniformly dispersed MXene and nanocellulose were injected as spinning dispersions from a syringe into a coagulation bath to obtain composite fibers with excellent performance. Mechanical and electrical properties can be precisely modulated through strategic adjustments of fiber diameter, alignment density, and MXene loading content. This technique demonstrates unique advantages in constructing MXene-based conductive frameworks, producing continuous ultrafine MXene/nanocellulose composite fibers with structural features mimicking natural extracellular matrices (fiber diameter: 50-500 nm). The resultant fibers exhibit superior porosity (85-98%), excellent pore interconnectivity (average pore size 2-15 μm), and exceptionally high specific surface area (up to 350 $m^2/g$) (**Figure 8(e)**) [183]. He *et al.* [184] developed nacre-inspired Co/C-modified CNF/MXene microfibers via wet spinning, achieving exceptional EMI SE of ≈62 dB in the

X-band (**Figure 8(f)**). Unlike impregnation deposition or spray coating, wet spinning enables precise control over MXene/CNF composite fiber, resulting in enhanced EMI shielding and mechanical properties. Direct fabrication of CNF/MXene composites into textile fibers allows subsequent weaving into fabrics or non-woven materials. These materials combine flexibility, breathability, and outstanding EMI shielding performance, making them ideal for wearable smart devices and protective clothing. The porous structure of the fabrics promotes multiple reflections and absorption of electromagnetic waves, thereby improving overall EMI SE. Post-treatments such as superhydrophobic modification can further impart water resistance and anti-fouling properties, extending material lifespan.

**4.2 2D layered structures**

MXene-based layered or composite film composites are widely applied in bulk materials and surface engineering, effectively mitigating the stacking issues inherent to 2D nanosheets [185]. In recent literature, flexible composite films have been emerged as promising candidates for foldable and wearable electronics [186,187]. The integration of MXene with robust nanocellulose through strong hydrogen bonding enables enhanced interfacial bonding within the composite matrix [188]. By regulating the mass ratio and interfacial interactions between nanocellulose and MXene, the mechanical properties, electrical conductivity, and microstructure of flexible composite films/papers can be precisely engineered. These flexible MXene/nanocellulose composite films or papers exhibit ultralight weight, ultrathin architectures, tunable thicknesses, prolonged durability, and straightforward fabrication processes, rendering them ideal for aerospace, biomedical, energy storage, and flexible sensing applications [189]. Ultrathin, lightweight, and flexible MXene/nanocellulose composites have been developed for EMI shielding applications, with

multifunctional integration including flame/water resistance, electrical insulation, breathability, self-cleaning, photothermal responsiveness, Joule heating capabilities, and pressure sensing [190]. These composites predominantly manifest as papers or composite films fabricated through vacuum filtration [191], dip coating [192], blade coating [193], and wet-milling blending (**Figures 9(a-c)**) [194]. Structural configurations are categorized as monolayer, Janus, or multilayer architectures based on stacking design.

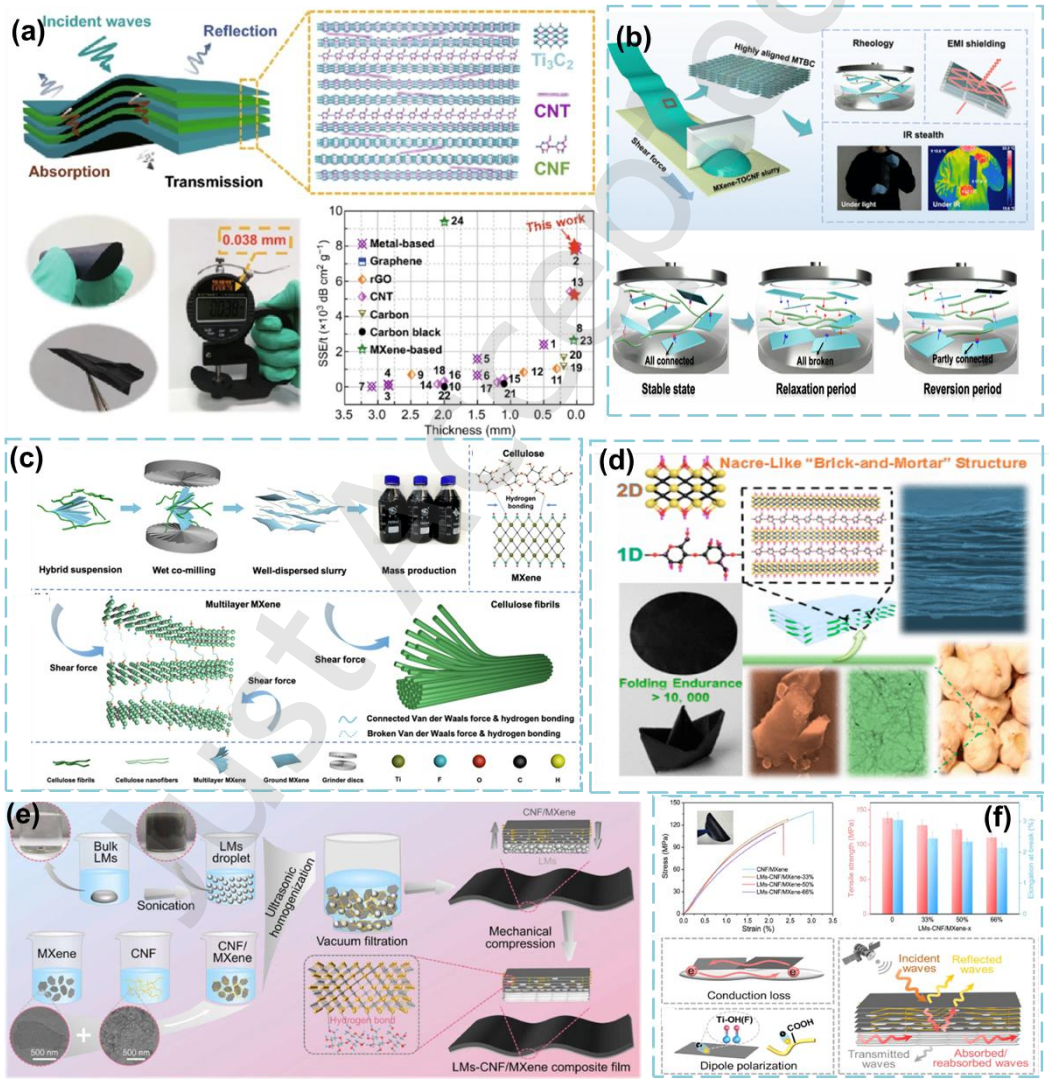


**Figure 9** Common methods for preparing electromagnetic shielding composites with 2D layered structures. (a) Vacuum filtration to form an electromagnetic shielding composite film with 38.4 dB EMI SE. Reproduced with permission from Ref. [191], © Cao, W. T. et al. 2019. (b) Large-scale preparation of MXene-TOCNF composite films by blade coating method. Reproduced with permission from Ref. [193], © American Chemical Society 2022. (c) For the fabrication of well-dispersed GMC Schematic representation of the wet co-grinding strategy of slurries for mass

production. Reproduced with permission from Ref. [194], © Elsevier Ltd. 2022. (d) Preparation of single-layer electromagnetic shielding composite film by vacuum filtration. Reproduced with permission from Ref. [33], © Cao, W. T. et al. 2018. (e) Electromagnetic shielding composite films with bilayer structure. (f) Applications and mechanical properties of electromagnetic shielding composite films. Reproduced with permission from Ref. [195], © Elsevier Ltd. 2025.

**Monolayer composite films.** Monolayer composite films usually have the advantages of easy preparation, stable properties, high degree of order, and large-scale preparation of homogeneous monolayers, in addition to monolayers are also easy to surface chemical modification and so on [196]. Notably, vacuum filtration remains a predominant method for preparing composite films with high viscosity. For instance, our group reported a vacuum-filtered MXene/CNF composite paper with nacre-inspired "brick-and-mortar" microstructure, achieving an EMI SE of 25.8 dB at 12.4 GHz that satisfies commercial requirements [33,197]. The $Ti_3C_2T_x$/CNF homogeneous composite film fabricated via hybrid filtration exhibited superior mechanical robustness with a tensile strength of 135.4 MPa and fracture strain of 16.7%. This composite film demonstrated exceptional folding endurance, sustaining 14,260 folding cycles without structural failure. Crucially, the 47 μm-thick uniform composite film maintains consistent electromagnetic shielding performance throughout mechanical stress testing, confirming structural-electrical stability (**Figure 9d**). Cao *et al.* [198] fabricated CNF/MXene/MCHS@Ag composite films via vacuum filtration using a 1:1 mass ratio of CNF:MXene. The MXene ensures high electrical conductivity, CNFs optimize dispersion and mechanical performance, while MCHS@Ag improves impedance matching and enhances wave absorption. Their synergistic interaction elevates the absorption-dominant SE (SEA contribution: 81%), overcoming limitations of conventional reflection-based shields, ultimately achieving 32.83 dB at 12.4 GHz - exceeding the commercial

threshold (>30 dB). Beyond this, monolayer composite films can be readily fabricated via blade-coating techniques—a strategy enabling scalable production of large-area, high-performance MXene-based composite films through solution processing. For instance, Feng *et al.* [199] employed doctor-blade coating to fabricate expansive (500 $cm^2$) MXene/TEMPO-TOCNF composite films with highly aligned and densely packed architectures. Owing to synergistic reinforcement from robust interfacial interactions and the compact aligned structure, these composite films demonstrated remarkable tensile strength of 281.7 MPa, Young's modulus of 14.87 GPa, and exceptional electrical conductivity of 46,685.3 $S \cdot m^{-1}$. Notably, the ordered microstructure and outstanding conductivity endowed the composite films with an electromagnetic shielding effectiveness of 50.2 dB and superior infrared stealth performance.

**Multilayered composite film.** Compared to monolayer or bilayer composite films, MXene/nanocellulose multilayer composite films demonstrate exceptional EMI shielding performance through tailored structural design and synergistic effects. Based on interlayer arrangement and functional engineering, MXene/nanocellulose multilayers are categorized into sandwich architectures [200], LBL assemblies [201], and other structures [16,63,202].

Sandwich architectures represent prevalent multilayer composite film structures that often exhibit multifunctional synergies. For instance, Cao *et al*. [191] fabricated a gradient-sandwich carbon nanotube/MXene/CNF paper via alternating vacuum filtration. The structure delivers high tensile strength (97.9 ± 5.0 MPa), fracture strain (4.6 ± 0.2%), conductivity (2506.6 $S \cdot m^{-1}$), and an EMI SE of 38.4 dB by modulating reflection-absorption contributions. Zhao *et al.* [195] fabricated Janus-structured LM-sandwiched CNF/MXene composite films through vacuum filtration-assisted gravitational deposition. The unique Janus architecture establishes an

"absorption-reflection-reabsorption" shielding mechanism, achieving exceptional EMI SE of 51.9 dB at ~27 μm thickness with a reduced reflection coefficient (0.89)-lower than conventional MXene-based shielding composite films (**Figures 9(e-f)**). Furthermore, employing a synergistic design strategy combining electrical conductivity gradients with sandwich architecture, Liang *et al.* [203] fabricated high-performance polyimide-MXene-multiwalled carbon nanotube nanocomposite composite films via precisely controlled electrospinning-spray assembly. The sandwich architectures strategically leverage the polyimide matrix, endowing the composite film with exceptional multifunctional properties. This nanocomposite maintains high-efficiency EMI shielding (66.8 dB) under extreme conditions while simultaneously exhibiting superior thermal insulation (30.5 $mW \cdot m^{-1} \cdot K^{-1}$) and flame retardancy.

The LBL structure is designed to achieve conductivity gradients by adjusting the MXene content of each layer, as well as the number of stacked layers. Exemplifying this approach, Lu *et al.* developed a high-performance MXene/nanocellulose composite film via spray-assisted LBL assembly [204]. By depositing MXene/CNF hybrid inks onto BC substrates through multiscale structural modulation and interfacial interaction control, they achieved densely packed lamellar architectures. The resulting composite films simultaneously deliver exceptional electromagnetic shielding (60 dB), electro-thermal conversion, and photo-thermal deicing functionalities. This methodology provides durable multifunctional composites particularly valuable for electromagnetic protection and ice mitigation in arctic/alpine electronics, power systems, and telecommunications infrastructure. In contrast, Chu *et al.* [205] fabricated laminated composite films via sequential filtration of separately blended MXene/CNF and h-PANI/CNF, achieving 35.3 dB. The alternating conductive/non‑ conductive layers enhance EMW attenuation through

impedance mismatch- induced multi- scattering and absorption [206]. Leveraging the inherent advantages of textile substrates, Wang *et al.* [207] constructed a tripartite architecture (PDA adhesion layer, MXene interlayer, hydrophobic topcoat) on textile substrates via LBL assembly. After four dip- coating cycles, the 45 μm sandwich- structured composite film delivered an EMI SE of 32 dB and a record SSE/t of 4085.92 $cm^2 \cdot g^{-1}$. For example, Da *et al.* [188] used alternate vacuum- assisted filtration followed by hot- pressing (150 °C, 12 MPa, 80 min) to produce a 12 μm Zn@MXene/CNF composite film, achieving 60.3 dB and an SE/t of 5025 $dB \cdot cm^{-1}$. $Zn^{2+}$ intercalation provided 30- day oxidation stability, and heterogeneous interfacial polarization between CNF and Zn@MXene further boosted absorption.

In addition, there are many innovations and advantages in other structures aimed at mimicking different objects in daily life to achieve different material properties and requirements. Under low packing load, randomly dispersed conductive additives cannot penetrate, thereby affecting the EMI shielding effect [208]. To overcome this, researchers have turned to biomimetic designs that regulate multiscale organization, interfacial distribution, and porosity, enhancing scattering/absorption and prolonging propagation paths [209,210]. Such structural control promotes electromagnetic wave scattering/absorption while prolonging propagation paths, thereby significantly improving shielding performance. Liu *et al.* [211]developed an ultrathin, flexible, and highly conductive Ag NW-doped $Ti_3C_2T_x$/CNF composite film through a facile vacuum-assisted filtration process that constructs bionic vein-like scaffolds. Within the leaf-like conductive network, electron migration and hopping contribute significantly to ohmic and dielectric losses across the dipole-rich surfaces of $Ti_3C_2T_x$ nanosheets. In addition, our group developed hollow metal-organic framework/MXene/CNF alternating electromagnetic structure

composite films using vacuum-deposition, demonstrating 66.8 dB shielding in GHz range and unprecedented 114.6 dB performance in THz frequencies [39]. Other structures tend to have continuous conductive paths along the alignment direction, which results in significantly higher shielding efficacy than the perpendicular direction, but requires precise control of the orientation process. Inspired by the ultra-spaced corrugated layer in cardboard, Wei *et al* [212] developed a novel composite paper with analogous corrugated architecture through the assembly of two modified cellulose sheets and an aerogel composite film. This configuration forms a standard Fabry-Pérot resonant cavity ('conductive layer-insulating layer-conductive layer'), facilitating electromagnetic wave energy attenuation. With a thickness of 0.6678 mm and MXene loading of 6.9 wt%, the composite paper achieved an exceptional EMI SE of 71.0 dB. Furthermore, it demonstrated superior infrared stealth capabilities, effectively masking human body thermal signatures. Remarkably, these infrared shielding properties remained robust even at elevated temperatures up to 120 °C. Guided by component selection and multilayer structural design principles, Wei *et al.* [213] synthesized an 'egg-box' architecture composite film comprising AgNPs, carbon spheres, MXene, and CNF. The fabrication involved immobilizing AgNPs onto hydrothermally carbonized cellulose microspheres—serving as sacrificial templates—to create 'egg'-like AgNPs@carbon spheres. Integration of high-aspect-ratio flexible CNFs with highly conductive MXene formed the box framework, significantly enhancing the composite film's mechanical robustness. This distinctive hierarchical design simultaneously prevented MXene restacking while expanding interlayer spacing, thereby generating abundant interfaces for electromagnetic wave reflection/scattering and promoting absorption efficiency. The resultant composite film achieved a tensile strength of 74.38 MPa with exceptional electromagnetic

shielding effectiveness of 74.53 dB. This systematic approach provides insights for designing tunable electromagnetic composites, significantly expanding MXene-based material applications.

**4.3 3D network architectures**

The inherent tendency of MXene nanosheets to form dense stacking due to van der Waals forces poses challenges in constructing 3D conductive pathways [214]. Biomimetic strategies involving hierarchical porous architectures effectively mitigate MXene sheet aggregation, enabling the nanoscale establishment of synergistic conductive-dielectric dual networks that significantly enhance charge carrier mobility and electromagnetic wave dissipation capacity [68]. Notably, 3D MXene-based gel systems (transition metal carbide/nitride derivatives) supported by nanocellulose frameworks demonstrate revolutionary potential in intelligent electromagnetic shielding applications, owing to their unique interfacial coupling effects and multiscale structural tunability. The 3D network architectures have many advantages, including high specific surface area, high porosity, good chemical resistance, low density, and light weight, which are suitable for electronic and communication devices that require miniaturization and high integration [15,35]. In addition, the porous structure can also promote impedance matching on the surface of the material and enhance the ability to absorb and dissipate electromagnetic waves inside the material, which is beneficial for electromagnetic shielding [7,215]. Based on morphological characteristics and fabrication methods, these systems are classified into hydrogels, foams and aerogels, each exhibiting distinct structural designs, performance attributes, and applications [216].

**Foams and aerogels**. Porous low-density nanostructured materials such as aerogels have been extensively developed. Nanocelluloses are commonly employed as conductive networks while simultaneously dispersing/stabilizing MXene nanosheets and enhancing interfacial polarization

between fillers [121]. Constructing porous $Ti_3C_2T_x$ architectures represent an effective strategy to enhance electromagnetic shielding by promoting multiple internal reflections and multiscale scattering events within the material [217,218]. To maximize electromagnetic wave energy dissipation through these mechanisms while minimizing reflective loss, the engineering of $Ti_3C_2T_x$ foams and aerogels has been extensively investigated [219-221]. One of the primary methods for fabricating 3D functional foams and aerogels is freeze-drying, also known as ice templating or freeze casting. In this process, a mixed MXene/nanocellulose suspension is injected or cast into a glass mold and frozen. During freezing, the water in the suspension forms ice crystals, causing the MXene/nanocellulose to rearrange under the directional growth of these ice crystals. The frozen sample is then transferred to a freeze dryer, where the ice crystals sublime into water vapor, leaving behind a MXene/nanocellulose composite that retains the porous structure [222]. Freeze-drying enables the formation of porous structures within the material, helping to maintain a high specific surface area. It ensures uniform distribution of nanocellulose and MXene throughout the composite while preserving its structural integrity. However, the method suffers from drawbacks including being time-consuming, costly, and energy-intensive. Additionally, structural changes may occur during preparation, potentially affecting the material's performance. In MXene/nanocellulose hybrid aerogels, the interaction between MXene and nanocellulose facilitates the formation of integrated porous structures, attributing to hydroxyl-mediated crosslinking [223]. The enhanced electromagnetic shielding performance of ultralight aerogels originates from synergistic effects between 1D nanocellulose and 2D MXene nanosheets. Compared to the multilayer architecture of composite films, the honeycomb-like morphology of porous aerogels generates additional internal scattering interfaces, distributing incident

electromagnetic radiation throughout the shielding layer to induce extra attenuation through combined absorption and reflection losses [35]. Mai *et al*. [39] fabricated a composite aerogels comprising zeolitic imidazolate framework-derived hollow CoNi carbon nanocages, MXene $Ti_3C_2T_x$, and CNF via a two-step freeze-drying strategy, demonstrating excellent electromagnetic shielding performance. The aerogels have good EMI SE with the characteristics of low reflection (35.1 dB with R coefficient = 0.28, and 21.2 dB with R coefficient = 0.25). Shi *et al*. [224] co-assembled MXene and CNF by directional freeze-drying, and then encapsulated a thin layer of flame-retardant PDMS onto the aerogel to construct a series of high-performance CNF/MXene/PDMS composite aerogels in a multilayer structure. The composite aerogels achieved ultra-high EMI SE of 96.8 dB and utilization efficiency of 1713.27 dB g $g^{-1}$. In addition, the PDMS coating effectively imparted excellent compressibility and durability to the 3D scaffolds, resulting in a compressive strength of 17.01 kPa, which was 199.5 percent higher than that of the CNF aerogel.

In addition to freeze-drying, cross-linking and 3D printing are also significant methods for fabricating 3D EMI shielding composites. Chen *et al*. [225] utilized 3D printing technology to prepare lightweight nanocellulose/MXene composite aerogel scaffolds with tunable EMI shielding performance. Fabricated via direct ink writing 3D printing, the composite scaffolds feature a multiscale 3D conductive network spanning macro-to-micro porous structures. They demonstrate optimal EMI SE of approximately 110 dB in the X-band, surpassing most as-reported EMI shielding materials. Furthermore, these scaffolds maintain EMI SE exceeding 45 dB across the ultra-wideband (UWB) GHz range (8.2-40 GHz). The design flexibility of 3D printing enables customized shielding components matching the size and geometry of protected electronics,

significantly advancing applications in miniaturized portable devices and EMI shielding solutions.

**Hydrogels**. Compared with aerogels, hydrogels exhibit higher density, micrometer-scale pores, and superior ductility [226]. The hydrogel system uses the combined water molecules as the dielectric response medium, combining the advantages of 3D porous frame with the coordinated hole constrained dielectric loss mechanism: the porous structure induces waveguide resonance of electromagnetic waves, while the highly polar confined water molecules dissipate electromagnetic energy through dipole-oriented polarization relaxation. Wei *et al.* [36] developed a multifunctional bioinspired hydrogel inspired by metal-ion chelation in mussel adhesive proteins. By dynamically crosslinking PAA and CNFs with $Ca^{2+}$ ions and incorporating conductive $Ti_3C_2T_x$ MXene nanosheets, they constructed a 3D networked hydrogel. This hydrogel demonstrates rapid self-healing (<1 s), ultrahigh stretchability (1000% strain), and biocompatibility (cell viability >93.7%). Its electrical resistance exhibits quadratic strain dependence (Gauge factor = 2.16), enabling applications in voice recognition, signature detection, and Morse code transmission. The synergistic effect of MXene conductive network and porous structure creates a heterogeneous interface between MXene and insulating PAA/CNF matrix, which enhances dielectric loss through interface polarization under alternating electric field. The 2 mm thick hydrogel has achieved 30dB EMI shielding in X-band, and has achieved complete performance recovery after healing. For example, Zhang *et al.* [227] integrated MXene@CNF Add nano fillers to polyacrylamide/gelatin matrix and optimize dynamic ion crosslinking induced by $CaCl_2$. The hydrogel exhibits excellent extensibility (>1600%), self-adhesiveness (17.4 kPa), frost resistance (-20 °C) and high sensitivity, and is suitable for flexible electronic skin and multi-mode sensing. The synergistic effect of 3D CNF network and MXene layered structure enhances the

absorption/reflection of electromagnetic waves, achieving an EMI SE of 33.8 dB.

**Table 2.** Comparison of mechanical and EMI shielding performance of representative MXene/nanocellulose composites

| Structure | Fabrication method | Electrical conductivity ($S \cdot m^{-1}$) | Mechanical property | EMI SE (dB) | Ref. |
|---|---|---|---|---|---|
| 2D composite film | Vacuum filtration | – | Tensile strength: 135.4 MPa Fracture strain: 16.7% | 25.8 | [33] |
| 2D composite film | Doctor-blade coating | 46,685.3 | Tensile strength: 281.7 MPa Young's modulus: 14.87 GPa | 50.2 | [199] |
| 2D composite film | Vacuum filtration | – | Tensile strength: 48.8 MPa | 32.83 | [198] |
| 2D composite film (Janus) | Vacuum filtration + gravitational deposition | 1911.1 | Tensile strength： 110.3 MPa | 51.9 (R=0.89) | [195] |
| 2D composite film (sandwich) | Alternating vacuum filtration | 2,506.6 | Tensile strength: 97.9 MPa Fracture strain: 4.6% | 38.4 | [191] |
| 2D composite film (sandwich) | Electrospinning | – | Breaking strength: 26.7 MPa | 60.8 | [189] |
| 2D composite film (LBL) | Spray coating | – | Tensile strength: > 250 MPa | 60 | [204] |

| | | | | | |
|---|---|---|---|---|---|
| 2D composite film (LBL) | Sequential filtration | ~1000 | Tensile strength: 24.45 MPa | 35.3 | [205] |
| 2D composite film (Bionics) | Vacuum filtration | 2743.6 | – | 66.8 | [211] |
| 2D composite film (Bionics) | Assembly by layers | 1000 | – | 71.0 | [212] |
| 2D composite film (Bionics) | Assembly by layers | 5900 | Tensile strength: 74.38 MPa | 74.38 | [213] |
| 3D foam/aerogel | Directional freeze-drying + PDMS coating | – | Compressive strength: 17.01 kPa (at 50% strain) | 96.8 | [224] |
| 3D foam/aerogel | 3D printing (direct ink writing) | ~900 | – | ~110 | [225] |
| 3D foam/aerogel | 3D printing (direct ink writing) | 282.14 | – | 54.01 | [228] |
| 3D foam/aerogel | Directional freeze-drying | – | Compressive stress: 62.2 kPa (at 50% strain) | 51.6 | [220] |
| 3D hydrogel | Dynamic crosslinking ($Ca^{2+}$, PAA/CNF) | – | Stretchability: > 1000% strain Self-healing: <1 s | 33.8 | [36] |

Comprehensive analysis based on **Table 2** reveals that the shielding and mechanical performances of MXene/nanocellulose composites vary significantly with structural morphology. Leveraging dense, layered stacking and a bio-inspired "brick-and-mortar" network, 2D composite films achieve a synergy of high tensile strength and superior electrical conductivity. Although they

deliver exceptional shielding efficiency, the mechanism is reflection-dominated, and the composite films suffer from poor air permeability and limited large-deformation capability. In contrast, 3D foams and aerogels shift the shielding mechanism toward absorption-dominated attenuation through highly porous architectures, offering the advantages of ultralow density and low secondary reflection. However, they exhibit lower mechanical strength and require energy-intensive fabrication processes. Meanwhile, 3D hydrogels utilize their three-dimensional networks and dynamic crosslinking to endow the materials with remarkable tensile strain, rapid self-healing capability, and environmental responsiveness, though their moderate shielding efficiency and environmental stability remain critical bottlenecks.

Consequently, structural selection necessitates a meticulous trade-off among mechanical strength, shielding mechanisms, flexibility, and processability. Specifically, 2D composite films are ideally suited for wearable electronics and aerospace applications, 3D aerogels are optimal for stealth technologies and lightweight scenarios, and hydrogels hold great potential for smart sensing and dynamic protection fields.

**Figure 10** compares the key advantages and limitations of 1D fibers, 2D composite films, 3D foams/aerogels, and 3D hydrogel architectures in MXene/nanocellulose composites, summarizing their distinct differences in mechanical strength, electrical conductivity, shielding performance, processability, and application suitability. 1D fibers offer high flexibility and breathability, yet they suffer from limited electrical conductivity and challenges in achieving large-scale uniformity. 2D composite films exhibit superior mechanical strength, high conductivity, and outstanding EMI shielding efficiency (e.g., greater than 50 dB); however, they are prone to MXene restacking and possess poor air permeability. 3D foams/aerogels achieve absorption-dominated shielding

alongside an ultralow density, but their freeze-drying fabrication process is energy-intensive and often results in low mechanical strength. 3D hydrogels feature exceptional stretchability, rapid self-healing capability, and favorable biocompatibility, though their environmental stability and thickness remain limiting factors. This comparative overview provides clear guidelines for selecting the appropriate MXene/nanocellulose morphology tailored for targeted applications in EMI shielding and flexible electronics.


**Figure 10.** Comparison of four typical MXene/nanocellulose structural systems (1D fibers, 2D composite films, 3D foams/aerogels, and 3D hydrogels).



## 5 Current challenges and future directions of MXene/nanocellulose composites

Although MXene/nanocellulose composites have made rapid progress in EMI shielding applications, there are still some challenges in the next step. To our knowledge, the future development direction of MXene/nanocellulose composites in EMI shielding is as follows:

1) Improving the environmental and health concerns related to MXene synthesis, and

shortcomings of nanocellulose. In the literature, numerous efforts have been reported [229]. For example, molten salt etching is developed for the synthesis of MXene, which have obviously advantages compared traditional etching method [230]. 2) Optimizing the structural design, stability, and scalability of MXene/nanocellulose composites. From an industrial perspective, combining roll‐to‐roll processing with doctor‐blade coating offers a straightforward and scalable route for continuous production of large‐area MXene/nanocellulose composite films, which can be directly integrated into existing coating lines for flexible electronics. For environmental stability, surface encapsulation with hydrophobic polymers (e.g., PDMS) or interlayer crosslinking (e.g., borate ions or polyelectrolytes) can effectively prevent MXene oxidation and moisture ingress, maintaining long-term shielding performance. For dynamic controllability, integrating stimuli‐responsive polymers (e.g., thermosensitive PNIPAM or electroactive hydrogels) into the composite enables real‐time tunability of EMI shielding effectiveness. Electromagnetic shielding involves multiple mechanisms, such as reflection, absorption, and conduction of electromagnetic waves. The shielding mechanisms of different MXene/nanocellulose composites with various structures are complex. In the literature, polyelectrolyte hydrogel encapsulated MXene has been developed to achieve absorption-dominated shielding in the X-band (absorption >90%) with humidity environmental stability >120 h using a combined aqueous layer to block oxygen and enhance polarization loss [231]. 3) Exploring synergistic toughening mechanisms of MXene/nanocellulose composites. In the low frequency range, electromagnetic waves are mainly manifested as magnetic waves. In the high frequency range, the wavelength of electromagnetic waves is relatively short, and the shielding effect mainly depends on the conductivity and surface structure of composites.

Composites with high conductivity perform better in the high frequency range, while composites with high magnetic permeability perform better in the low frequency range [232]. Iron-based ferrites, particularly those composed of $Fe_2O_3$ combined with transition metals (e.g., Ni, Ba, Co), have emerged as highly promising microwave-absorbing materials due to their excellent ferromagnetic properties. Currently, a 3D magnetic MXene/$Fe_3O_4$@MWCNT composite aerogel was fabricated via directional freeze-drying [220]. Hydrogen bonding and van der Waals interactions between $Fe_3O_4$@MWCNT and hydrophilic MXene nanosheets endowed the structure with excellent stability under 60% strain. Simultaneously, the uniformly dispersed $Fe_3O_4$ nanoparticles on MWCNT effectively prevented magnetic agglomeration while achieving ultralow density (10 $mg \cdot cm^{-3}$) and high absorption power coefficient (0.69), ultimately delivering an electromagnetic shielding effectiveness of 51.6 dB. 4) Balancing the weight, thickness, flexibility, and corrosion resistance of MXene/nanocellulose composites while pursuing higher EMI SE. For instance, an ultralight biomimetic shielding aerogel with excellent shielding effect and good mechanical flexibility was designed [35], which has a density of only 8.0 $mg/cm^3$, along with an excellent electromagnetic shielding value of 74.6 dB. Ultra-thin CNFs were utilized to co-construct an ultra-low density MXene aerogel with oriented bionic pore walls, which meets the lightweight requirement for electromagnetic shielding composites. To achieve a balanced performance, we suggest using performance indices such as SSE/t (specific shielding effectiveness per thickness) and applying multi‑ objective optimization strategies to guide material design. 5) Improving environmental adaptability of MXene/nanocellulose composites. The performance of MXene/nanocellulose electromagnetic shielding composites in specific environments, such as high temperature, high humidity, high salt, and strong solar radiation, lacks in-depth research.

These environmental factors may cause damage for the composites and reduce its EMI SE. For example, a cellulose composite paper was developed with a three-layer protective structure: an outer TOCNF/cationic starch hydrogel composite film, a middle TOCNF/MXene pearl layer, and an inner conductive layer [233]. The introduction of a PDMS encapsulation layer enabled the composite paper to maintain more than 90% EMI SE in hot and humid environments. Beyond encapsulation, crosslinking MXene with nanocellulose via covalent bonds (e.g., silane coupling agents) or metal ion intercalation (e.g., $Zn^{2+}$) can enhance long-term resistance to moisture and oxygen. 6) Extending broadband electromagnetic shielding performance of MXene/nanocellulose composites. Electromagnetic waves have a wide frequency range, and electromagnetic waves of different frequencies have different shielding characteristics. How to design structures and components to achieve effective wideband shielding is a scientific challenge in current electromagnetic shielding research [234]. Currently, the composite films were prepared consisting of hollow metal-organic frameworks/layered MXene/nanocellulose with a unique alternating electromagnetic structure [39]. The as-optimized composite film exhibited excellent EMI shielding performance of 66.8 dB at GHz and 114.6 dB at THz. To further broaden the effective frequency range, we recommend constructing gradient or multilayer architectures that combine different loss mechanisms (e.g., magnetic loss from ferrites at low frequencies and dielectric loss from MXene at high frequencies). 7) Dynamic controlling electromagnetic shielding of MXene/nanocellulose composites. With the rapid development of wireless communication and IoT devices, electromagnetic radiation is ubiquitous, and traditional static MXene/nanocellulose electromagnetic shielding composites are unable to meet the dynamic shielding requirements [235,236]. How to use MXene/nanocellulose composites to achieve dynamic control

of electromagnetic wave response is a fundamental scientific challenge. In the literature, Meng's team prepared PMCP hydrogels by constructing MXene/carbon nanotubes (MXene-CNTs) thermoreceptor networks in temperature-sensitive hydrogels (PVA/PNIPAM) [237]. The dynamic reconstruction of the gel network caused by temperature rise independently adapts to the interface resistance of the MXene/CNTs conductive network, resulting in a third-order adjustable EMI SE that changes with temperature. Therefore, MXene/CNT-PNIPAM thermosensitive hydrogel with optically controlled EMI SE switch (9.3-53.9 dB) was prepared, which can adjust the electromagnetic shielding switch through temperature.

**6 Conclusion**

In summary, we reviewed the latest research progress in the development of MXene/nanocellulose composites for electromagnetic shielding applications. This review article focuses on various preparation strategies used in the synthesis of MXene/nanocellulose composites, ranging from simple mixing methods to more complex *in-situ* manufacturing techniques. These methods are crucial for optimizing the distribution and interaction between MXene and nanocellulose, which ultimately determines the effectiveness of composites in EMI shielding. In addition, we also explored the toughening mechanisms of these composites, which play a key role in improving their mechanical properties without compromising their electromagnetic properties. The synergistic effect of MXene's metallic conductivity and nanocellulose reinforcement structure endows the composites with excellent mechanical integrity, flexibility, and electromagnetic shielding effect. In addition, the structural design of composites has always been a key focus, striving to manipulate the arrangement, dispersion, and morphology of MXene and nanocellulose to achieve optimal EMI shielding while maintaining or even

enhancing the strength and toughness of the composites.

EMI shielding performance of MXene/nanocellulose composites originates from three fundamental mechanisms: reflection, absorption, and multiple internal reflections. The high electrical conductivity of the MXene network favors reflection, whereas the abundant interfaces between MXene and nanocellulose induce interfacial polarization, thereby dissipating electromagnetic energy. Furthermore, porous configurations (such as aerogels and foams) facilitate multiple scattering and internal absorption, enabling absorption-dominated shielding with low secondary radiation. Key factors for enhancing shielding performance include tuning the MXene-to-cellulose ratio to optimize impedance matching, incorporating magnetic components to achieve magneto-dielectric synergy, and constructing polarization centers via defect engineering or heteroatom doping. These insights demonstrate that MXene/nanocellulose composites represent highly promising candidates for high-performance, flexible, and lightweight EMI shielding materials.

Despite these advances, the large-scale preparation of MXene/nanocellulose composites and their potential applications in electromagnetic shielding still face some challenges. Further research is needed on the scalability of manufacturing technology, the long-term stability of composites under different environmental conditions, and the repeatability of their shielding performance on an industrial scale. In addition, it is necessary to carefully evaluate the environmental impact and cost-effectiveness of these composites to ensure their practical industrial application. However, it is expected that MXene/nanocellulose composites will play a key role in the development of advanced materials for electromagnetic interface shielding in the near future. It is expected that MXene/nanocellulose composites will be widely applied and

developed in the field of electromagnetic shielding.

**Acknowledgements**

This work was supported by the National Natural Science Foundation of China (22478036).

**Declaration of Competing Interest**

The authors declare that they have no known competing financial interests or personal relationships that could have appeared to influence the work reported in this paper.

**Data availability**

No datasets were generated or analyzed during the current study.

**Author information**

**Corresponding Author**

Ming-Guo Ma − Research Center of Biomass Clean Utilization, MOE Engineering Research Center of Forestry Biomass Materials and Bioenergy, College of Materials Science and Technology, Beijing Forestry University, Beijing 100083, PR China.

*E-mail: mg_ma@bjfu.edu.cn

**ORCID**

Ming-Guo Ma: 0000-0001-6319-9254

## References


[1] Liu, A.; Qiu, H.; Lu, X.H.; Guo, H.; Hu, J.W.; Liang, C.B.; He, M.K.; Yu, Z.; Zhang, Y.L.; Kong, J.; Gu, J.W. Asymmetric structural MXene/PBO aerogels for high-performance electromagnetic interference shielding with ultra-low reflection. *Adv. Mater.* **2025,** 37, 2414085.

[2] Zhang, Y.L.; Ruan, K.P.; Zhou, K.; Gu, J.W. Controlled distributed $Ti_3C_2T_x$ hollow microspheres on thermally conductive polyimide composite films for excellent electromagnetic interference shielding. *Adv. Mater.* **2023,** 35, 2211642.

[3] Yan, R.H.; Lin, Q.H.; You, K.J.; Zhang, L.; Chen, Y.; Huang, Z.; Sheng, X.X. Construction strategies and recent advances of flexible EMI phase change composites. *Soft Sci.* **2025,** 5, 8.

[4] Liu, Y.; Liu, Y.; Zhao, X. MXene composite electromagnetic shielding materials: the latest research status. *ACS Appl. Mater. Interfaces.* **2024,** 16, 41596-41615.

[5] Li, X.; Huang, Z.; Shuck, C.E.; Liang, G.; Gogotsi, Y.; Zhi, C. MXene chemistry, electrochemistry and energy storage applications. *Nat. Rev. Chem.* **2022,** 6, 389-404.

[6] Wang, L.; Cheng, J.; Zou, Y.; Zheng, W.; Wang, Y.; Liu, Y.; Zhang, H.; Zhang, D.; Ji, X. Current advances and future perspectives of MXene-based electromagnetic interference shielding materials. *Adv. Compos. Hybrid Mater.* **2023,** 6, 172.

[7] Shahzad, F.; Alhabeb, M.; Hatter, C.B.; Anasori, B.; Hong, S.M.; Koo, C.M.; Gogotsi, Y. Electromagnetic interference shielding with 2D transition metal carbides (MXenes). *Science* **2016,** 353, 1137-1140.

[8] Iqbal, A.; Shahzad, F.; Hantanasirisakul, K.; Kim, M.-K.; Kwon, J.; Hong, J.; Kim, H.; Kim, D.; Gogotsi, Y.; Koo, C.M. Anomalous absorption of electromagnetic waves by 2D transition metal carbonitride $Ti_3CNT_x$ (MXene). *Science* **2020,** 369, 446-450.

[9] Zhou, X.F.; Min, P.; Liu, Y.; Jin, M.; Yu, Z.Z.; Zhang, H.B. Insulating electromagnetic-shielding silicone compound enables direct potting electronics. *Science* **2024,** 385, 1205-1210.

[10] Liang, C.B.; Qiu, H.; Zhang, Y.L.; Liu, Y.Q.; Gu, J.W. External field-assisted techniques for polymer matrix composites with electromagnetic interference shielding. *Sci. Bull.* **2023,** 68, 1938-1953.

[11] Li, Y.; Wang, Y.; Huang, Y. A Review on MXene/nanocellulose composites: toward wearable multifunctional electromagnetic interference shielding application. *Small.* **2025,** 21, 2410283.

[12] Seyedian, S.M.; Ghaffari, A.; Mirkhan, A.; Ji, G.; Tan, S.; Ghorbanian-Gezaforodi, S.; Peymanfar, R. Manipulating the phase and morphology of $MgFe_2O_4$ nanoparticles for promoting their optical, magnetic, and microwave absorbing/shielding characteristics. *Ceram. Int.* **2024,** 50, 13447-13458.

[13] Nezafat, Z.; Jafari, G.; Javanshir, S.; Peymanfar, R. MXene-based metal oxide/metal composites for microwave absorption and shielding: recent advances and future perspectives. *Adv. Compos. Hybrid Mater.* **2025,** 8, 447.

[14] Dogari, H.; Ghafuri, H.; Peymanfar, R. Ultrathin microwave absorbing structures at the k-band from PDA-implanted CNTs, doped conjugated carbon using peganum harmala seeds and turpentine derivatives. *Adv. Sustain. Syst.* **2025,** 9, 2400793.

[15] Wang, J.; Ming, W.; Chen, L.; Song, T.; Yele, M.; Zhang, H.; Yang, L.; Sarula, G.; Liang, B.; Yan, L.; Wang, G. $MoS_2$ lubricate-toughened MXene/ANF composites for multifunctional electromagnetic interference shielding. *Nano-Micro Lett.* **2024,** 17, 36.

[16] Ming, W.; Yang, L.; Chen, H.; Fei, F.; Zhang, H.; Sarula, G.; Wang, J.; Wang, T.; Jin, C.; Liang, B.; Zhang, L.; Yan, L. High toughness MXene/ANF-CZIF67/ANF "magnetic–electric" Janus film for

multifunctional low reflection electromagnetic interference shielding. *Nano Res.* **2025,** 18, 94907621.
[17] Wang, J.; Song, T.; Ming, W.; Yele, M.; Chen, L.; Zhang, H.; Zhang, X.; Liang, B.; Wang, G. High MXene loading, nacre-inspired MXene/ANF electromagnetic interference shielding composite films with ultralong strain-to-failure and excellent Joule heating performance. *Nano Res.* **2024,** 17, 2061-2069.
[18] Yele, M.; Sarula, G.; Yang, J.; Yang, L.; Zhang, H.; Chen, L.; Zhang, X.; Wang, J.; Wang, T.; Jin, C.; Liang, B.; Yan, L. Integrated structural-functional MXene-GNs/ANF flexible composite film with enhanced thermal conductivity and electromagnetic interference shielding performance. *J. Mater. Sci. Technol.* **2026,** 241, 200-210.
[19] Meng, Y.; Cai, B.; Zhou, Y.; Zhou, L.; Zhang, Y.; Wang, J.; Sarula, G.; Yan, L.; Lu, M.; Liang, B.; Wang, G. Bionic coral reef inspired enhanced scattering of trimetallic LDH self assembled $Ti_3C_2T_x$ MXene for advanced microwave absorption. *Nano Res.* **2025,** 18, 94907842.
[20] Guo, W.Y.; Li, C.; Ji, X.X.; Ma, M.G. A critical review of MXene/nanocellulose composite films. *Ind. Crop. Prod.* **2023,** 206, 117609.
[21] Wang, L.; Lang, L.; Hu, X.; Gao, T.; He, M.; Qiu, H.; Ji, X.; Guo, H.; Zhang, Y.; Huang, S. Multifunctional ionic bonding-strengthened ($Ti_3C_2T_x$ MXene/CNF)-(BNNS/CNF) composite films with Janus structure for outstanding electromagnetic interference shielding and thermal management. *J. Mater. Sci. Technol.* **2025,** 224, 46-55.
[22] Thomas, B.; Raj, M.C.; Athira, K.B.; Rubiyah, M.H.; Joy, J.; Moores, A.; Drisko, G.L.; Sanchez, C. Nanocellulose, a versatile green platform: from biosources to materials and their applications. *Chem. Rev.* **2018,** 118, 11575-11625.
[23] Liu, Y.; Wang, Y.D.; Wu, N.; Han, M.R.; Liu, W.; Liu, J.R.; Zeng, Z.H. Diverse structural design strategies of MXene-based macrostructure for high-performance electromagnetic interference shielding. *Nano-Micro Lett.* **2023,** 15, 240.
[24] Liu, Q.; Wang, P.L.; Zhang, W.; Mai, T.; Qi, M.Y.; Chen, L.; Li, J.F.; Ma, M.G. Multifunctional wood-derived cellulose/Ti3C2Tx composite films enhanced by densification strategy for electromagnetic shielding, Joule/solar heating, and thermal camouflage. *Chem. Eng. J.* **2024,** 493, 152696.
[25] Ma, C.; Ma, M.G.; Si, C.L.; Ji, X.X.; Wan, P.B. Flexible MXene-based composites for wearable devices. *Adv. Funct. Mater.* **2021,** 31, 2009524.
[26] Li, W.; Zhou, T.; Zhang, Z.; Li, L.; Lian, W.; Wang, Y.; Lu, J.; Yan, J.; Wang, H.; Wei, L.; Cheng, Q. Ultrastrong MXene film induced by sequential bridging with liquid metal. *Science* **2024,** 385, 62-68.
[27] Zhang, W.; Ji, X.X.; Ma, M.G. Emerging MXene/cellulose composites: design strategies and diverse applications. *Chem. Eng. J.* **2023,** 458, 141402.
[28] Saito, T.; Kimura, S.; Nishiyama, Y.; Isogai, A. Cellulose nanofibers prepared by TEMPO-mediated oxidation of native cellulose. *Biomacromolecules* **2007,** 8, 2485-2491.
[29] Saito, T.; Nishiyama, Y.; Putaux, J.L.; Vignon, M.; Isogai, A. Homogeneous suspensions of individualized microfibrils from TEMPO-catalyzed oxidation of native cellulose. *Biomacromolecules* **2006,** 7, 1687-1691.
[30] Naguib, M.; Kurtoglu, M.; Presser, V.; Lu, J.; Niu, J.J.; Heon, M.; Hultman, L.; Gogotsi, Y.; Barsoum, M.W. Two-dimensional nanocrystals produced by exfoliation of $Ti_3AlC_2$. *Adv. Mater.* **2011,** 23, 4248-4253.
[31] Zhu, X.L.; Liu, B.C.; Hou, H.J.; Huang, Z.Y.; Zeinu, K.M.; Huang, L.; Yuan, X.Q.; Guo, D.B.; Hu, J.P.; Yang, J.K. Alkaline intercalation of $Ti_3C_2$ MXene for simultaneous electrochemical detection of

Cd(II), Pb(II), Cu(II) and Hg(II). *Electrochim. Acta.* **2017,** 248, 46-57.
[32] Yarbrough, J.M.; Zhang, R.; Mittal, A.; Vander Wall, T.; Bomble, Y.J.; Decker, S.R.; Himmel, M.E.; Ciesielski, P.N. Multifunctional cellulolytic enzymes outperform processive fungal cellulases for coproduction of nanocellulose and biofuels. *ACS Nano* **2017,** 11, 3101-3109.
[33] Cao, W.T.; Chen, F.F.; Zhu, Y.J.; Zhang, Y.G.; Jiang, Y.Y.; Ma, M.G.; Chen, F. Binary strengthening and toughening of MXene/cellulose nanofiber composite paper with nacre-inspired structure and superior electromagnetic interference shielding properties. *ACS Nano* **2018,** 12, 4583-4593.
[34] Cao, W.T.; Ouyang, H.; Xin, W.; Chao, S.Y.; Ma, C.; Li, Z.; Chen, F.; Ma, M.G. A stretchable highoutput triboelectric nanogenerator improved by MXene liquid electrode with high electronegativity. *Adv. Funct. Mater.* **2020,** 30, 2004181.
[35] Zeng, Z.H.; Wang, C.X.; Siqueira, G.; Han, D.X.; Huch, A.; Abdolhosseinzadeh, S.; Heier, J.; Nüesch, F.; Zhang, C.F.; Nyström, G. Nanocellulose-MXene biomimetic aerogels with orientation-tunable electromagnetic interference shielding performance. *Adv. Sci.* **2020,** 7, 2000979.
[36] Wei, J.J.; Zhu, C.L.; Zeng, Z.H.; Pan, F.; Wan, F.Q.; Lei, L.W.; Nyström, G.; Fu, Z.Y. Bioinspired cellulose-integrated MXene-based hydrogels for multifunctional sensing and electromagnetic interference shielding. *Interdiscip. Mater.* **2022,** 1, 495-506.
[37] Mai, T.; Guo, W.Y.; Wang, P.L.; Chen, L.; Qi, M.Y.; Liu, Q.; Ding, Y.; Ma, M.G. Bilayer metal-organic frameworks/MXene/nanocellulose paper with electromagnetic double loss for absorption-dominated electromagnetic interference shielding. *Chem. Eng. J.* **2023,** 464, 142517.
[38] He, Y.Q.; Yang, J.; Chen, W.T.; Chen, W.; Zhao, L.; Qi, W. Gallium-doped MXene/cellulose nanofiber composite membranes with electro/photo thermal conversion property for high performance electromagnetic interference shielding. *Chem. Eng. J.* **2023,** 464, 142565.
[39] Mai, T.; Chen, L.; Wang, P.-L.; Liu, Q.; Ma, M.-G. Hollow metal–organic framework/MXene/nanocellulose composite films for giga/terahertz electromagnetic shielding and photothermal conversion. *Nano-Micro Lett.* **2024,** 16, 169.
[40] Liu, M.X.; Zhang, H.R.; Huang, X.M.; Zhang, Z.Y.; Zhang, K.L.; Chen, Z.W.; Zhou, J.T.; Pan, L. An electric-magnetic dual-gradient composite film comprising MXene, hollow $Fe_3O_4$, and bacterial cellulose for high-performance EMI shielding and infrared camouflage. *Adv. Funct. Mater.* **2025,** 35, 2419077.
[41] Qin, R.Z.; Nong, J.; Wang, K.Q.; Liu, Y.S.; Zhou, S.B.; Hu, M.J.; Zhao, H.B.; Shan, G.C. Recent Advances in Flexible Pressure Sensors Based on MXene Materials. *Adv. Mater.* **2024,** 36, 2419077.
[42] Huo, Q.Q.; Liang, C.B.; Qi, J.M.; He, M.K.; Si, X.F.; Xue, F.P.; Qiu, H.; Gu, J.W. Bioinspired asymmetric janus film enables concurrent dynamic infrared camouflage and electromagnetic interference shielding. *Adv. Funct. Mater.* **2026,** 36, e22330.
[43] Amara, U.; Hussain, I.; Ahmad, M.; Mahmood, K.; Zhang, K.L. 2D MXene-based biosensing: a review. *Small* **2023,** 19, 2205249.
[44] Hu, X.F.; Zhang, Y.L.; Guo, H.; He, M.K.; Qiu, H.; Shi, X.T.; Wang, L.; Gu, J.W. Multifunctional flexible WPU composite aerogels with sandwich structure for dual-sided low-reflection electromagnetic interference shielding. *Adv. Funct. Mater.* **2026,** 36, e17665.
[45] Wu, Y.Y.; Li, W.; Ren, Q.Y.; Li, J.Z.; Xu, W.; Xu, J. First-principles study on adsorption of gas molecules by metal Sc modified $Ti_2CO_2$. *Acta Phys. Sin.* **2024,** 73, 073101.
[46] Niu, R.; Han, R.; Wang, Y.; Zhang, L.; Qiao, Q.; Jiang, L.; Sun, Y.; Tang, S.; Zhu, J. MXene-based porous and robust 2D/2D hybrid architectures with dispersed $Li_3Ti_2(PO_4)_3$ as superior anodes for

lithium-ion battery. *Chem. Eng. J.* **2021,** 405, 127049.
[47] Lang, J.-Q.; Chen, L.; Ji, X.-X.; Liu, Q.; Ma, M.-G. Triboelectric nanogenerators for thermal management application: current progress and future prospects. *Nano-Micro Lett.* **2026,** 18, 274.
[48] Cheng, Y.; Lyu, W.H.; Wang, Z.H.; Ouyang, H.; Zhang, A.J.; Sun, J.X.; Yang, T.; Fu, B.; He, B.Q. MXenes: synthesis, incorporation, and applications in ultrafast lasers. *Nanotechnology* **2021,** 32, 392003.
[49] Lang, J.-Q.; Li, C.; Chen, L.; Liu, Q.; Wan, W.; Yang, H.-Y.; Ma, M.-G. Cellulose nanofiber/boron nitride/MXene ternary composite films with excellent thermal conductivity for high output triboelectric nanogenerators under high temperature. *Chem. Eng. J.* **2025,** 522, 167292.
[50] Xu, C.; Wang, L.B.; Liu, Z.B.; Chen, L.; Guo, J.K.; Kang, N.; Ma, X.L.; Cheng, H.M.; Ren, W.C. Large-area high-quality 2D ultrathin $Mo_2C$ superconducting crystals. *Nat. Mater.* **2015,** 14, 1135-1141.
[51] Wang, D.; Zhou, C.K.; Filatov, A.S.; Cho, W.J.; Lagunas, F.; Wang, M.Z.; Vaikuntanathan, S.; Liu, C.; Klie, R.F.; Talapin, D.V. Direct synthesis and chemical vapor deposition of 2D carbide and nitride MXenes. *Science* **2023,** 379, 1242-1247.
[52] Liang, L.L.; Gu, W.H.; Wu, Y.; Zhang, B.S.; Wang, G.H.; Yang, Y.; Ji, G.B. Heterointerface engineering in electromagnetic absorbers: new insights and opportunities. *Adv. Mater.* **2022,** 34, 2106195.
[53] Dogari, H.; Peymanfar, R.; Ghafuri, H. Microwave absorbing characteristics of porphyrin derivates: a loop of conjugated structure. *RSC Adv.* **2023,** 13, 22205-22215.
[54] Sheykhmoradi, S.; Ghaffari, A.; Mirkhan, A.; Ji, G.B.; Tan, S.J.; Peymanfar, R. Dendrimer-assisted defect and morphology regulation for improving optical, hyperthermia, and microwave-absorbing features. *Dalton Trans.* **2024,** 53, 4222-4236.
[55] Urbančič, J.; Shi, H.; Nia, A.S.; Pavlica, E. Semiconducting polymer-MXene blends with improved charge carrier mobilities and their application in field-effect transistors. *Mater. Lett. X* **2025,** 25, 100244.
[56] Wang, Y.; Pan, J.; Zhang, Y.; Ma, T.; Zhao, J.; Zhang, L.; Yan, M.; Zhang, S. High-efficiency electrospun PVDF@MXene composite membrane with covalent bonding and well-dispersed internal materials for solar-driven seawater desalination. *Desalination* **2024,** 592, 118146.
[57] Li, L.; Wang, B.; Hubler, M.H. Carbon nanofibers (CNFs) dispersed in ultra-high performance concrete (UHPC): Mechanical property, workability and permeability investigation. *Cem. Concr. Compos.* **2022,** 131, 104592.
[58] Xu, W.B.; Yang, Y.R.; Wang, Y.Z.; Zhang, Y.L.; Li, T.H.; Liu, A.; Gong, W.; Gu, J.W. Polymer-based composite fibers for electromagnetic interference shielding. *Susmat* **2026**, 6, e70071.
[59] Al-Fakih, G.O.A.; Ilyas, R.A.; Atiqah, A.; Atikah, M.S.N.; Saidur, R.; Dufresne, A.; Saharudin, M.S.; Abral, H.; Sapuan, S.M. Advanced functional materials based on nanocellulose/MXene: A review. *Int. J. Biol. Macromol.* **2024,** 278, 135207.
[60] Yang, Y.; Luo, C.-L.; Chen, X.-D.; Wang, M. Sustainable electromagnetic shielding graphene/nanocellulose thin films with excellent joule heating and mechanical properties via in-situ mechanical exfoliation and crosslinking with cations. *Compos. Sci. Technol.* **2023,** 233, 109913.
[61] Zhou, B.; Li, Q.T.; Xu, P.H.; Feng, Y.Z.; Ma, J.M.; Liu, C.T.; Shen, C.Y. An asymmetric sandwich structural cellulose-based film with self-supported MXene and AgNW layers for flexible electromagnetic interference shielding and thermal management. *Nanoscale* **2021,** 13, 2378-2388.
[62] Wang, X.; Guo, J.; Ren, H.; Jin, J.; He, H.; Jin, P.; Wu, Z.; Zheng, Y. Research progress of nanocellulose-based food packaging. *Trends Food Sci. Technol.* **2024,** 143, 104289.

[63] Lu, W.; Zhou, Y.; Xu, H. Dual-gradient MXene/AgNWs/hollow-$Fe_3O_4$/CNF composite films for thermal management and electromagnetic shielding applications. *Compos. Commun.* **2024,** 51, 102077.
[64] Chang, Y.K.; Li, P.H.; Li, L.; Chang, S.P.; Huo, Y.J.; Mu, C.P.; Nie, A.M.; Xiang, J.Y.; Xue, T.Y.; Zhai, K.; Wang, B.C.; Zhao, Z.S.; Yu, D.L.; Wen, F.S.; Liu, Z.Y.; Tian, Y.J. In situ grown ultrafine $RuO_2$ nanoparticles on $GeP_5$ nanosheets as the electrode material for flexible planar micro-supercapacitors with high specific capacitance and cyclability. *ACS Appl. Mater. Interfaces.* **2021,** 13, 47560-47571.
[65] Cao, W.T.; Ma, C.; Mao, D.S.; Zhang, J.; Ma, M.G.; Chen, F. MXene-reinforced cellulose nanofibril inks for 3D-printed smart fibres and textiles. *Adv. Funct. Mater.* **2019,** 29, 1905898.
[66] Chen, L.; Mai, T.; Guo, Z.-H.; Liu, Q.; Lang, J.-Q.; Ma, M.-G. 3D-printed MXene-based gradient framework for enhanced anti-reflection performance and excellent electromagnetic interference shielding with multi-scene adaptability. *Chem. Eng. J.* **2025,** 513, 162871.
[67] Song, Q.C.; Zhan, Z.Y.; Chen, B.X.; Zhou, Z.H.; Lu, C.H. Biotemplate synthesis of polypyrrole@bacterial cellulose/MXene nanocomposites with synergistically enhanced electrochemical performance. *Cellulose* **2020,** 27, 7475-7488.
[68] Asghar, A.; Rashid, M.S.; Hanif, M.; Boukhris, I.; Chen, Z.; Saqib, M.; Arshad, Q.; Rosaiah, P.; Ali, S.; Hussain, I. Advancements in MXene-based 3D printing-based technologies. *Chem. Eng. J.* **2025,** 506, 159811.
[69] Guan, X.M.; Yang, Z.H.; Zhu, Y.T.; Yang, L.J.; Zhou, M.; Wu, Y.; Yang, L.; Deng, T.W.; Ji, G.B. The controllable porous structure and s-doping of hollow carbon sphere synergistically act on the microwave attenuation. *Carbon.* **2022,** 188, 1-11.
[70] Chen, G.; Zhang, L.M.; Luo, B.C.; Wu, H.J. Optimal control of the compositions, interfaces, and defects of hollow sulfide for electromagnetic wave absorption. *J. Colloid Interface Sci.* **2022,** 607, 24-33.
[71] Zhang, Y.; Zhang, G.C.; Ma, Z.L.; Qin, J.B.; Shen, X. Heterogeneous MXene-based films with graded electrical conductivity towards highly efficient EMI shielding and electrothermal heating. *Nano Res.* **2024,** 17, 7264-7274.
[72] Sagadevan, S.; Fatimah, I.; Lett, J.A.; Kakavandi, B.; Soga, T.; Oh, W.C.; Randriamahazaka, H. Exploring the potential of MXene-based aerogels and hybrid nanocomposites for supercapacitor applications. *J. Energy Storage.* **2024,** 99, 113269.
[73] Lang, J.-Q.; Li, C.; Chen, L.; Mai, T.; Guo, Z.-H.; Ma, M.-G. A polyethyleneimine-functionalized cellulose nanofiber/MXene composite aerogel: Towards highly efficient adsorption of crude oil, organic solvents, and dyes. *J. Water Process Eng.* **2025,** 74, 107808.
[74] Li, S.; Luo, L.; Hasan, M.Z.; Shi, N.; Liu, Q.; Li, D.; Yue, C.; Zhang, R.; Sha, S.; Zhu, J. Directional fabrication of an ultra-light and porous bacterial nanocellulose/MXene composite aerogel for efficient thermal management. *Int. J. Biol. Macromol.* **2025,** 311, 144054.
[75] Tang, S.; Wu, Z.; Li, X.; Xie, F.; Ye, D.; Ruiz-Hitzky, E.; Wei, L.; Wang, X. Nacre-inspired biodegradable nanocellulose/MXene/AgNPs films with high strength and superior gas barrier properties. *Carbohydr. Polym.* **2023,** 299, 120204.
[76] Huang, X.; Tuersun, Y.; Luo, P.J.; Yang, H.R.; Chu, S. In-situ reduction of AgNPs on MXene surfaces for synthesis of efficient thermally conductive composites with powerful electromagnetic shielding capabilities. *Colloid Surface A.* **2023,** 677, 132444.
[77] Geng, Y.; Chen, H.; Luo, S.; Teng, Y.; He, Q.; Zhang, L.; Zhang, Z.; Yang, Z.; Shi, Y.; Wang, Q.; Yang, J.; Fan, J.; Yang, Y. In-Situ formed Titanium-MXene nanomembrane as ultrathin van-der-Waals

lubricant. *Mater. Today.* **2025**, 88, 328-337.
[78] Hu, Y.; Chen, Z.; Ding, Y.; Xu, Y.; Lin, H.; Yu, W.; Teng, J.; Shen, L.; Jiao, Y.; Liao, B.-Q. Nanofiltration membranes fabricated by plant polyphenol-intermediated MXene and polyethyleneimine layer-by-layer self-assembly for efficient dye/salt separation. *Sep. Purif. Technol.* **2023,** 323, 124343.
[79] Shang, Y.; Ji, Y.; Dong, J.; Yang, G.; Zhang, X.; Su, F.; Feng, Y.; Liu, C. Sandwiched cellulose nanofiber /boron nitride nanosheet /$Ti_3C_2T_x$ MXene composite film with high electromagnetic shielding and thermal conductivity yet insulation performance. *Compos. Sci. Technol.* **2021,** 214, 108974.
[80] Li, J.; Xia, F.; Liu, Y.; Wang, J.; Su, X.; Li, Z.; Peng, H. Synthesis of MXene-based functional coatings on rigid polyurethane foam surfaces: A comparative study of layer-by-layer self-assembly and hydrothermal methods. *Polym. Degrad. Stab.* **2024,** 220, 110665.
[81] Zhang, H.; Zhang, X.; Qiu, C.; Jia, P.; An, F.; Zhou, L.; Zhu, L.; Zhang, D. Polyaniline/ZnO heterostructure-based ammonia sensor self-powered by electrospinning of PTFE-PVDF/MXene piezo-tribo hybrid nanogenerator. *Chem. Eng. J.* **2024,** 496, 154226.
[82] Qiu, D.; Zheng, K.; Guan, T.; Li, Z.; Peng, J.; Tao, Q.; Yan, K.; Bao, N. Wet spinning of MXene ($V_2CT_X$) based fiber fabric with high electrochemical performance for flexible supercapacitor. *J. Alloys Compd.* **2024,** 991, 174230.
[83] Liu, L.; Chen, W.; Zhang, H.; Zhang, Y.; Tang, P.; Li, D.; Deng, Z.; Ye, L.; Yu, Z. Tough and electrically conductive $Ti_3C_2T_x$ MXene–based core–shell fibers for high–performance electromagnetic interference shielding and heating application. *Chem. Eng. J.* **2022,** 430, 133074.
[84] Wu, Z.C.; Cheng, H.W.; Jin, C.; Yang, B.T.; Xu, C.Y.; Pei, K.; Zhang, H.B.; Yang, Z.Q.; Che, R.C. Dimensional design and core-shell engineering of nanomaterials for electromagnetic wave absorption. *Adv. Mater.* **2022,** 34, 2107538.
[85] Wu, Y.; Zhao, Y.; Zhou, M.; Tan, S.J.; Peymanfar, R.; Aslibeiki, B.; Ji, G.B. Ultrabroad microwave absorption ability and infrared stealth property of nano-micro CuS@rGO lightweight aerogels. *Nano-Micro Lett.* **2022,** 14, 171.
[86] Peymanfar, R.; Mousivand, P.; Mirkhan, A. Fabrication of ZnS/g-$C_3N_4$/Gypsum plaster nanocomposite toward refining electromagnetic pollution and saving energy. *Energy Technol.* **2024,** 12, 2300684.
[87] Zhang, H.B.; Cheng, J.Y.; Wang, H.H.; Huang, Z.H.; Zheng, Q.B.; Zheng, G.P.; Zhang, D.Q.; Che, R.C.; Cao, M.S. Initiating VB-group laminated $NbS_2$ electromagnetic wave absorber toward superior absorption bandwidth as large as 6.48 GHz through phase engineering modulation. *Adv. Funct. Mater.* **2022,** 32, 2108194.
[88] Nan, Z.; Wei, W.; Lin, Z.; Ouyang, J.; Chang, J.; Hao, Y. Flexible electromagnetic interference shields: Materials, structure and multifunctionalization. *Mater. Sci. Eng. R.* **2024,** 160, 100823.
[89] Nan, Z.; Wei, W.; Lin, Z.; Chang, J.; Hao, Y. Flexible nanocomposite conductors for electromagnetic interference shielding. *Nano-Micro Lett.* **2023,** 15, 172.
[90] Wu, Q.; Zeng, Z.; Xiao, L. From 2D graphene and MXene nanolayers to 3D biomimetic porous composite aerogels for electromagnetic interference shielding. *Compos. Part A Appl. Sci. Manuf.* **2024,** 177, 107939.
[91] Zuo, S.; Liang, Y.; Yang, H.; Ma, X.; Ge, S.; Wu, Y.; Fei, B.; Guo, M.; Ahamad, T.; Le, H.S.; Le, Q.V.; Xia, C. High strength composites of carbon fiber sheets-veneers sandwich-structure for electromagnetic interference shielding materials. *Prog. Org. Coat.* **2022,** 165, 106736.
[92] Lyu, J.; Zhao, X.; Hou, X.; Zhang, Y.; Li, T.; Yan, Y. Electromagnetic interference shielding based

on a high strength polyaniline-aramid nanocomposite. *Compos. Sci. Technol.* **2017,** 149, 159-165.
[93] Cheng, J.; Li, C.; Xiong, Y.; Zhang, H.; Raza, H.; Ullah, S.; Wu, J.; Zheng, G.; Cao, Q.; Zhang, D.; Zheng, Q.; Che, R. Recent Advances in design strategies and multifunctionality of flexible electromagnetic interference shielding materials. *Nano-Micro Lett.* **2022,** 14, 80.
[94] Zhang, Y.; Ruan, K.; Gu, J. Flexible sandwich-structured electromagnetic interference shielding nanocomposite films with excellent thermal conductivities. *Small* **2021,** 17, 2101951.
[95] Zhang, D.; Yin, R.; Zheng, Y.; Li, Q.; Liu, H.; Liu, C.; Shen, C. Multifunctional MXene/CNTs based flexible electronic textile with excellent strain sensing, electromagnetic interference shielding and Joule heating performances. *Chem. Eng. J.* **2022,** 438, 135587.
[96] Wu, N.; Zeng, Z.; Kummer, N.; Han, D.; Zenobi, R.; Nyström, G. Ultrafine cellulose nanofiber-assisted physical and chemical cross-linking of MXene sheets for electromagnetic interference shielding. *Small Methods* **2021,** 5, 2100889.
[97] Li, B.; Wu, N.; Yang, Y.; Pan, F.; Wang, C.; Wang, G.; Xiao, L.; Liu, W.; Liu, J.; Zeng, Z. Graphene Oxide-assisted multiple cross-linking of MXene for large-area, high-strength, oxidation-resistant, and multifunctional films. *Adv. Funct. Mater.* **2023,** 33, 2213357.
[98] Verma, R.; Thakur, P.; Chauhan, A.; Jasrotia, R.; Thakur, A. A review on MXene and its' composites for electromagnetic interference (EMI) shielding applications. *Carbon.* **2023,** 208, 170-190.
[99] Tang, H.; Wang, R.; Shi, L.; Sheremet, E.; Rodriguez, R.D.; Sun, J. Post-processing strategies for improving the electrical and mechanical properties of MXenes. *Chem. Eng. J.* **2021,** 425, 131472.
[100] Guo, P.; Su, L.; Jia, S.; Ni, Z.; Dai, Z.; Guo, J.; Wang, X.; Peng, K.; Wang, H. Strong SiC@Carbon nanowire aerogel metamaterials for efficient electromagnetic interference shielding. *Carbon.* **2024,** 229, 119492.
[101] Xie, D.; Zhang, R.; Song, S.; Yang, S.; Yang, A.; Zhang, C.; Song, Y. Nacre-inspired starch-based bioplastic with excellent mechanical strength and electromagnetic interference shielding. *Carbohydr. Polym.* **2024,** 331, 121888.
[102] Han, X.; Qiu, X.; Zong, M.; Hao, J. Assembled MXene Macrostructures for Multifunctional Polymer Nanocomposites. *Small Struct.* **2023,** 4, 2300090.
[103] Cao, H.; Neal, N.N.; Pas, S.; Radovic, M.; Lutkenhaus, J.L.; Green, M.J.; Pentzer, E.B. Architecting MXenes in polymer composites. *Prog. Polym. Sci.* **2024,** 153, 101830.
[104] Heng, W.; Weihua, L.; Bachagha, K. Review on design strategies and applications of flexible cellulose‐ carbon nanotube functional composites. *Carbohydr. Polym.* **2023,** 321, 121306.
[105] Moon, R.J.; Martini, A.; Nairn, J.; Simonsen, J.; Youngblood, J. Cellulose nanomaterials review: structure, properties and nanocomposites. *Chem. Soc. Rev.* **2011,** 40, 3941-3994.
[106] Chen, Z.; Hu, Y.; Shi, G.; Zhuo, H.; Ali, M.A.; Jamróz, E.; Zhang, H.; Zhong, L.; Peng, X. Advanced flexible materials from nanocellulose. *Adv. Funct. Mater.* **2023,** 33, 2214245.
[107] Mokhena, T.C.; Sadiku, E.R.; Mochane, M.J.; Ray, S.S.; John, M.J.; Mtibe, A. Mechanical properties of cellulose nanofibril papers and their bionanocomposites: A review. *Carbohydr. Polym.* **2021,** 273, 118507.
[108] Mahmoud, M.M.; Khaled, C.; and El Mogy, S.A. Nanocellulose: a comprehensive review of structure, pretreatment, extraction, and chemical modification. *Polym. Rev.* **2024,** 64, 1414-1475.
[109] Xue, G.B.; Liu, K.; Chen, Q.; Yang, P.H.; Li, J.; Ding, T.P.; Duan, J.J.; Qi, B.; Zhou, J. Robust and low-cost flame-treated wood for high-performance solar steam generation. *ACS Appl. Mater. Interfaces.* **2017,** 9, 15052-15057.
[110] Abdul Khalil, H.P.S.; Bhat, A.H.; Ireana Yusra, A.F. Green composites from sustainable

cellulose nanofibrils: A review. *Carbohydr. Polym.* **2012,** 87, 963-979.
[111]Zhang, Z.; Abidi, N.; Lucia, L.; Chabi, S.; Denny, C.T.; Parajuli, P.; Rumi, S.S. Cellulose/nanocellulose superabsorbent hydrogels as a sustainable platform for materials applications: A mini-review and perspective. *Carbohydr. Polym.* **2023,** 299, 120140.
[112] Aghvami-Panah, M.; Ameli, A. MXene/Cellulose composites as electromagnetic interference shields: Relationships between microstructural design and shielding performance. *Compos. Part A Appl. Sci. Manuf.* **2024,** 176, 107879.
[113] Dai, T.; Liu, Y.; Rong, D.; Wang, M.; Qi, Z.; Zhao, Y.; Wang, X.; Yang, Q.; Wei, L.; Chen, M. Bioinspired dynamic matrix based on developable structure of MXene-cellulose nanofibers (CNF) soft actuators. *Adv. Funct. Mater.* **2024,** 34, 2400459.
[114] Wan, Y.; Xiong, P.; Liu, J.; Feng, F.; Xun, X.; Gama, F.M.; Zhang, Q.; Yao, F.; Yang, Z.; Luo, H.; Xu, Y. Ultrathin, strong, and highly flexible $Ti_3C_2T_x$ MXene/bacterial cellulose composite films for high-performance electromagnetic interference shielding. *ACS Nano* **2021,** 15, 8439-8449.
[115] Liu, M.; Zhang, L.; Rostami, J.; Zhang, T.; Matthews, K.; Chen, S.; Fan, W.; Zhu, Y.; Chen, J.; Huang, M.; Wu, J.; Wang, H.; Hamedi, M.M.; Xu, F.; Tian, W.; Wågberg, L.; Gogotsi, Y. Tough MXene-cellulose nanofibril ionotronic dual-network hydrogel films for stable zinc anodes. *ACS Nano* **2025,** 19, 13399-13413.
[116] Zhai, M.; Zhao, S.; Guo, H.; Li, X.; Shi, X.; He, M.; Zhang, Y.; Gu, J. Bionic-structured electromagnetic interference shielding composites. *Sci. Bull.* **2025,** 70, 2347-2364.
[117] Qin, Z.; Chen, X.; Lv, Y.; Zhao, B.; Fang, X.; Pan, K. Wearable and high-performance piezoresistive sensor based on nanofiber/sodium alginate synergistically enhanced MXene composite aerogel. *Chem. Eng. J.* **2023,** 451, 138586.
[118] Haataja, R.; Myllymäki, S.; Laitinen, O.; Jantunen, H.; Liimatainen, H. Controlling the cell and surface architecture of cellulose nanofiber/PVA/$Ti_3C_2T_X$ MXene hybrid cryogels for optimized permittivity and EMI shielding performance. *Mater. Des.* **2023,** 228, 111855.
[119] Zhou, G.; Wang, X.; Wan, T.; Liu, C.; Chen, W.; Jiang, S.; Han, J.; Yan, Y.; Li, M.; Mei, C. Electrostatic self-assembly of $Ti_3C_2T_X$ MXene/cellulose nanofiber composite films for wearable supercapacitor and joule heater. *Energy Environ. Mater.* **2023,** 6, e12454.
[120] Hu, K.; Zhao, Z.; Wang, Y.; Yu, L.; Liu, K.; Wu, H.; Huang, L.; Chen, L.; Ni, Y. A tough organohydrogel-based multiresponsive sensor for a triboelectric nanogenerator and supercapacitor toward wearable intelligent devices. *J. Mater. Chem. A.* **2022,** 10, 12092-12103.
[121] Xu, T.; Song, Q.; Liu, K.; Liu, H.; Pan, J.; Liu, W.; Dai, L.; Zhang, M.; Wang, Y.; Si, C.; Du, H.; Zhang, K. Nanocellulose-assisted construction of multifunctional MXene-based aerogels with engineering biomimetic texture for pressure sensor and compressible electrode. *Nano-Micro Lett.* **2023,** 15, 98.
[122] Tian, L.; Gao, F.-L.; Li, Y.-X.; Yang, Z.-Y.; Xu, X.; Yu, Z.-Z.; Shang, J.; Li, R.-W.; Li, X. High-Performance bimodal temperature/pressure tactile sensor based on lamellar CNT/MXene/cellulose nanofibers aerogel with enhanced multifunctionality. *Adv. Funct. Mater.* **2025,** 35, 2418988.
[123] Zhang, F.; Ren, P.; Guo, Z.; Wang, J.; Chen, Z.; Zong, Z.; Hu, J.; Jin, Y.; Ren, F. Asymmetric multilayered MXene-AgNWs/cellulose nanofiber composite films with antibacterial properties for high-efficiency electromagnetic interference shielding. *J. Mater. Sci. Technol.* **2022,** 129, 181-189.
[124] Hong, X.; Du, Z.; Li, L.; Jiang, K.; Chen, D.; Shen, G. Biomimetic Honeycomb-like $Ti_3C_2T_X$ MXene/Bacterial cellulose aerogel-based flexible pressure sensor for the human–computer interface.

*ACS Sens.* **2025,** 10, 417-426.

[125] Zeng, Z.; Mavrona, E.; Sacré, D.; Kummer, N.; Cao, J.; Müller, L.A.E.; Hack, E.; Zolliker, P.; Nyström, G. Terahertz birefringent biomimetic aerogels based on cellulose nanofibers and conductive nanomaterials. *ACS Nano* **2021,** 15, 7451-7462.

[126] Tian, W.; VahidMohammadi, A.; Reid, M.S.; Wang, Z.; Ouyang, L.; Erlandsson, J.; Pettersson, T.; Wågberg, L.; Beidaghi, M.; Hamedi, M.M. Multifunctional nanocomposites with high strength and capacitance using 2D MXene and 1D nanocellulose. *Adv. Mater.* **2019,** 31, 1902977.

[127] Zhou, X.; Wen, J.; Ma, X.; Wu, H. Manipulation of microstructure of MXene aerogel via metal ions-initiated gelation for electromagnetic wave absorption. *J. Colloid Interface Sci.* **2022,** 624, 505-514.

[128] Zhang, Y.; Liu, A.; Tian, Y.; Tian, Y.; Qi, X.; Qiu, H.; He, M.; Zhou, K.; Gu, J. Direct-ink-writing printed aerogels with dynamically reversible thermal management and tunable electromagnetic interference shielding. *Adv. Mater.* **2025,** 37, 2505521.

[129] Qi, C.-Z.; Wu, X.; Liu, J.; Luo, X.-J.; Zhang, H.-B.; Yu, Z.-Z. Highly conductive calcium ion-reinforced MXene/sodium alginate aerogel meshes by direct ink writing for electromagnetic interference shielding and Joule heating. *J. Mater. Sci. Technol.* **2023,** 135, 213-220.

[130] Dong, B.; Yu, D.; Lu, P.; Song, Z.; Chen, W.; Zhang, F.; Li, B.; Wang, H.; Liu, W. TEMPO bacterial cellulose and MXene nanosheets synergistically promote tough hydrogels for intelligent wearable human-machine interaction. *Carbohydr. Polym.* **2024,** 326, 121621.

[131] Zhu, L.; Yang, H.; Xu, T.; Wang, L.; Lei, J.; Si, C. Engineered nanochannels in MXene heterogeneous proton exchange membranes mediated by cellulose nanofiber/sodium alginate dual crosslinked networks. *Adv. Funct. Mater.* **2025,** 35, 2419334.

[132] Tang, S.; Wu, Z.; Feng, G.; Wei, L.; Weng, J.; Ruiz-Hitzky, E.; Wang, X. Multifunctional sandwich-like composite film based on superhydrophobic MXene for self-cleaning, photodynamic and antimicrobial applications. *Chem. Eng. J.* **2023,** 454, 140457.

[133] Zhao, D.; Dang, L.-Y.; Wang, G.-G.; Sun, N.; Deng, X.; Han, J.-C.; Zhu, J.-Q.; Yang, Y. Multifunctional, superhydrophobic and highly elastic MXene/bacterial cellulose hybrid aerogels enabled via silylation. *J. Mater. Chem. A.* **2022,** 10, 24772-24782.

[134] Liu, A.; Xu, X.; Qiu, H.; Guo, H.; He, M.; Yu, Z.; Zhang, Y.; Gu, J. Bioinspired hollow heterostructure fillers for enhanced electromagnetic interference shielding in polyimide aerogels. *InfoMat.* **2025,** 7, e70060.

[135] Cai, C.; Zhang, L.; Meng, X.; Luo, B.; Liu, Y.; Chi, M.; Wang, J.; Liu, T.; Zhang, S.; Wang, S.; Nie, S. Mechanically robust triboelectric aerogels enabled by dense bridging of MXene. *Nano Lett.* **2024,** 24, 16022-16030.

[136] Chen, H.-; Chen, Z.Y.; Mao, M.; Wu, Y.Y.; Yang, F.; Gong, L.X.; Zhao, L.; Cao, C.F.; Song, P.; Gao, J.F.; Zhang, G.D.; Shi, Y.Q.; Cao, K.; Tang, L.C. Self-adhesive polydimethylsiloxane foam materials decorated with MXene/cellulose nanofiber interconnected network for versatile functionalities. *Adv. Funct. Mater.* **2023,** 33, 2304927.

[137] Wang, S.; Ma, Y.; Zhu, S.; Ma, H.; Yue, Y.; Wu, Q.; Xiao, H.; Han, J. Biomimetic and electrostatic self-assembled nanocellulose/MXene films constructed with sequential bridging strategy for flexible supercapacitor. *Chem. Eng. J.* **2024,** 495, 153552.

[138] Chen, J.; Chen, H.; Chen, M.; Zhou, W.; Tian, Q.; Wong, C.-P. Nacre-inspired surface-engineered MXene/nanocellulose composite film for high-performance supercapacitors and zinc-ion capacitors. *Chem. Eng. J.* **2022,** 428, 131380.

[139] Yang, L.; Cui, J.; Zhang, L.; Xu, X.; Chen, X.; Sun, D. A moisture-driven actuator based on polydopamine-modified MXene/bacterial cellulose nanofiber composite film. *Adv. Funct. Mater.* **2021,** 31, 2101378.

[140] Ni, Q.-Y.; He, X.-F.; Zhou, J.-L.; Yang, Y.-Q.; Zeng, Z.-F.; Mao, P.-F.; Luo, Y.-H.; Xu, J.-M.; Jiang, B.; Wu, Q.; Wang, B.; Qin, Y.-Q.; Gong, L.-X.; Tang, L.-C.; Li, S.-N. Mechanical tough and stretchable quaternized cellulose nanofibrils/MXene conductive hydrogel for flexible strain sensor with multi-scale monitoring. *J. Mater. Sci. Technol.* **2024,** 191, 181-191.

[141] Cai, C.; Wei, Z.; Huang, Y.; Fu, Y. Wood-inspired superelastic MXene aerogels with superior photothermal conversion and durable superhydrophobicity for clean-up of super-viscous crude oil. *Chem. Eng. J.* **2021,** 421, 127772.

[142] Pan, L.; Wang, H.; Zhou, J.; Dai, H.; Xu, H.; Guo, Y.; Cheng, T.; Yin, L.; Zhang, T.; Wang, Y.; Zhou, J.; Sun, G. Spinning dope modulation via ph-triggered multiscale sheet-wire linkages for constructing strong $Ti_3C_2T_X$ MXene fibers with high volumetric capacitance. *Adv. Funct. Mater.* **2025**, 35, 2505247.

[143] Yao, L.; Qian, L.; Song, W.; Zhang, S.; Zhang, Y.; Zhang, L.; Li, X.; Yan, G.; Nica, V. Advancements in $Ti_3C_2T_x$ MXene stability: synergistic antioxidant strategies and their impact on long-lasting flexible sensors. *ACS Appl. Mater. Interfaces.* **2024,** 16, 48147-48162.

[144] Zotov, V.; Vijjamarri, S.; Mousavi, S.-D.; Du, G., Poly(silyl ether)s as degradable and sustainable materials: synthesis and applications. *Molecules* **2024**, 29, 1498.

[145] Yang, Y.; Lu, Y.; Chen, L.; Jing, Y.; Zhang, K. Recyclable, highly thermally stable and intrinsically flame retardant bio-based polybenzoxazine vitrimers enabled by dual dynamic covalent bonds. *Angew. Chem. Int. Ed.* **2026,** 65, e8806571.

[146] Kong, F.; Li, J.; Hou, Z.; Liu, F.; Yao, M.; Li, Y.; Liu, K.; Zhang, F.; Yu, M.; Shen, H.; Li, J.; Yan, Z.; Jiao, L.; Chen, J.; Cheng, F. Polydopamine nanocages orchestrate multi-site networks on the $Ni_4Mo$ electrocatalyst for efficient and ultrastable hydrogen evolution. *J. Am. Chem. Soc.* **2026,** 148, 15771-15781.

[147] Lu, Z.; Bai, S.; Lu, H.; Zhu, Z.; Yu, J.; Wang, Q.; Zhang, P.; Qian, L.; Zheng, Z.; Yu, Y. Rapid photocontrollable dopamine polymerization for instant adaptive wet adhesion. *Nat. Commun.* **2026,** 16, 11150.

[148] Luo, S.; Xiang, T.; Dong, J.; Su, F.; Ji, Y.; Liu, C.; Feng, Y. A double crosslinking MXene/cellulose nanofiber layered film for improving mechanical properties and stable electromagnetic interference shielding performance. *J. Mater. Sci. Technol.* **2022,** 129, 127-134.

[149] Zhao, D.; Zhou, X.; Cui, T.; Wang, G.-G. Nanocellulose-assisted construction of multi-cavity structured $Ti_3C_2T_x$/melamine composite sponges for enhanced electromagnetic interference shielding. *Compos. Part A Appl. Sci. Manuf.* **2024,** 185, 108347.

[150] Fu, Y.; Li, C.; Cheng, Y.; He, Y.; Zhang, W.; Wei, Q.; Li, D. Biomass aerogel composite containing $BaTiO_3$ nanoparticles and MXene for highly sensitive self-powered sensor and photothermal antibacterial applications. *Compos. Part A Appl. Sci. Manuf.* **2023,** 173, 107663.

[151] Wang, H.; Han, P.; Yu, Y.; Han, S.; Qiao, Y.; Li, Y.; Sun, B.; Gu, Z. Multifunctional flexible MXene/TA@CNC electronic hydrogel patch with robust adhesion and self-healing properties for wearable electronics. *Chem. Eng. J.* **2025,** 507, 160329.

[152] Wei, Y.; Xiang, L.; Ou, H.; Li, F.; Zhang, Y.; Qian, Y.; Hao, L.; Diao, J.; Zhang, M.; Zhu, P.; Liu, Y.; Kuang, Y.; Chen, G. MXene-based conductive organohydrogels with long-term environmental stability and multifunctionality. *Adv. Funct. Mater.* **2020,** 30, 2005135.

[153] Qiao, J.; Song, Q.; Xuan, L.; Liu, J.; Zhang, X.; Zheng, S.; Lin, J.; Cai, W.; Zhang, Q.; Zeng, Z.; Wu, N. Dual cross-linked magnetic MXene aerogel with high strength and durability enables multifunctionality. *Adv. Funct. Mater.* **2024,** 34, 2401687.

[154] Ma, J.W.; Zeng, F.R.; Lin, X.C.; Wang, Y.Q.; Ma, Y.H.; Jia, X.X.; Zhang, J.C.; Liu, B.W.; Wang, Y.Z.; Zhao, H.B. A photoluminescent hydrogen-bonded biomass aerogel for sustainable radiative cooling. *Science* **2024,** 385, 68-74.

[155] Zhao, X.M.; Yang, Y.F.; Yin, X.M.; Luo, Z.; Chan, K.Y.; Shen, X. Size-insensitive vapor diffusion enabled by additive freeze-printed aerogels for scalable desalination. *ACS Energy Lett.* **2025,** 10, 3419-3429.

[156] Wu, N.; Yang, Y.; Wang, C.; Wu, Q.; Pan, F.; Zhang, R.; Liu, J.; Zeng, Z. Ultrathin cellulose nanofiber assisted ambient-pressure-dried, ultralight, mechanically robust, multifunctional MXene aerogels. *Adv. Mater.* **2023,** 35, 2207969.

[157] Cao, M.-S.; Shu, J.-C.; Wen, B.; Wang, X.-X.; Cao, W.-Q. Genetic dielectric genes inside 2D carbon-based materials with tunable electromagnetic function at elevated temperature. *Small Struct.* **2021,** 2, 2100104.

[158] Peymanfar, R.; Javanshir, S.; Naimi-Jamal, M.R.; Tavassoli, S.H. Morphology and medium influence on microwave characteristics of nanostructures: A review. *J. Mater. Sci.* **2021,** 56, 17457-17477.

[159] Fahimi, A.; Fakharian, P.; Mirakhan, A.; Farahani, A.; Zhou, Z.; Zhao, Y.; Peymanfar, R. Elemental doping and size effect-modified biomass-derived carbon: a fascinating microwave absorbing/shielding and energy saving material. *J. Mater. Chem. C* **2024,** 12, 12535-12548.

[160] Qin, R.; Li, T.; Tian, Y.; Zou, Y.; Liu, C.; Sun, J.; Qi, Q.; Meng, F. Dielectric-tuned hierarchical nanoarchitectures integrated with volatile corrosion inhibitor systems enable synergistic active-passive anti-corrosion and ultra-broadband microwave absorption. *Nano Res.* **2025,** 18, 94907740.

[161] Peymaneh, Z.; Sheykhmoradi, S.; Nezafat, Z.; Ghaffari, A.; Mirkhan, V.; Ghorbanian-Gezaforodi, S.; Peymanfar, R. Phase composition or material morphology, which one plays the pioneering role in promoting microwave absorption and hyperthermia. *Chem. Eng. J. Adv.* **2025,** 24, 100845.

[162] Sun, Z.; Tian, S.; Guo, Z.; Bi, J.; Wang, J.; Sha, Y.; Xie, H.; Qian, L. Multi-stage anisotropic cellulose-based aerogels via "foam-flake-fiber" interweaving for versatile microwave absorbers. *Adv. Funct. Mater.* **2025,** 35, 2508255.

[163] Peymanfar, R.; Selseleh-Zakerin, E.; Ahmadi, A.; Tavassoli, S.H. Architecting functionalized carbon microtube/carrollite nanocomposite demonstrating significant microwave characteristics. *Sci. Rep.* **2021,** 11, 11932.

[164] Rezaei, H.; Soltani-Mohammadi, F.; Dogari, H.; Ghafuri, H.; Peymanfar, R. Plasma-assisted doping of pyrolyzed corn husk strengthened by $MoS_2$/polyethersulfone for fascinating microwave absorbing/shielding and energy saving properties. *Nanoscale* **2024,** 16, 18962-18975.

[165] Yu, L.; Luo, S.; Yang, Y.; Huang, X.; Xiao, Y.; Chen, Q.; Fu, L.; Liu, R.; Xia, L.; Xue, Y. Robust multifunctional MXene-based composite films with Janus-like structure for high-performance electromagnetic interference shielding, electrothermal conversion and infrared stealth. *J. Alloys Compd.* **2026,** 1051, 186036.

[166] Mai, T.; Yang, S.-C.; Chen, L.; Lang, J.-Q.; Zhu, Y.-F.; Ma, M.-G. Sheep leather-inspired asymmetrical aerogel-film composites for low reflection electromagnetic wave shielding and rapid

photothermal conversion. *Carbon.* **2026,** 255, 121534.

[167] Mani, D.; Kim, S.-R. MXene/graphene fluoride/cellulose nanofiber gradient structure films for thermal management and electromagnetic interference shielding. *Mater. Today Commun.* **2025,** 44, 112043.

[168] Zhang, J.; Fu, S.; Liu, H.; Feng, B.; Yang, X.; Zhang, B. High wet-strength MXene/lignin-containing cellulose nanofibrils composite films with Janus structure for electromagnetic shielding and Joule heating. *Int. J. Biol. Macromol.* **2025,** 327, 147468.

[169] Hu, F.; Li, M.; Li, P.; Zeng, J.; Wang, T.; Li, J.; Wang, B.; Wu, C.; Chen, K. High-performance multifunctional nanopapers with superior mechanical strength, electromagnetic interference shielding, and thermal management for next-generation electronics. *Adv. Funct. Mater.* **2025,** 35, 2418899.

[170] Liu, D.; Gao, Y.; Song, Y.; Zhu, H.; Zhang, L.; Xie, Y.; Shi, H.; Shi, Z.; Yang, Q.; Xiong, C. Highly sensitive multifunctional electronic skin based on nanocellulose/MXene composite films with good electromagnetic shielding biocompatible antibacterial properties. *Biomacromolecules* **2022,** 23, 182-195.

[171] Ma, C.; Cao, W.-T.; Zhang, W.; Ma, M.-G.; Sun, W.-M.; Zhang, J.; Chen, F. Wearable, ultrathin and transparent bacterial celluloses/MXene film with Janus structure and excellent mechanical property for electromagnetic interference shielding. *Chem. Eng. J.* **2021,** 403, 126438.

[172] Baig, N.; Kammakakam, I.; Falath, W. Nanomaterials: a review of synthesis methods, properties, recent progress, and challenges. *Mater. Adv.* **2021,** 2, 1821-1871.

[173] Song, J.; Xu, K.; He, J.; Ye, H.; Xu, L. Three-dimensional graphene/carbon nanotube electromagnetic shielding composite material based on melamine resin foam template. *Polym. Compos.* **2023,** 44, 2836-2845.

[174] Han, M.; Shuck, C.E.; Rakhmanov, R.; Parchment, D.; Anasori, B.; Koo, C.M.; Friedman, G.; Gogotsi, Y. Beyond $Ti_3C_2T_x$: MXenes for electromagnetic interference shielding. *ACS Nano.* **2020,** 14, 5008-5016.

[175] Wang, Q.-W.; Zhang, H.-B.; Liu, J.; Zhao, S.; Xie, X.; Liu, L.; Yang, R.; Koratkar, N.; Yu, Z.-Z. Multifunctional and water-resistant MXene-decorated polyester textiles with outstanding electromagnetic interference shielding and joule heating performances. *Adv. Funct. Mater.* **2019,** 29, 1806819.

[176] Cheng, B.; Wu, P. Scalable Fabrication of kevlar/$Ti_3C_2T_x$ MXene intelligent wearable fabrics with multiple sensory capabilities. *ACS Nano* **2021,** 15, 8676-8685.

[177] Liu, Z.; Zhu, T.; Wang, J.; Zheng, Z.; Li, Y.; Li, J.; Lai, Y. Functionalized fiber-based strain sensors: pathway to next-generation wearable electronics. *Nano-Micro Lett.* **2022,** 14, 61.

[178] Liang, C.; Huo, Q.; Qi, J.; Zhang, Y.; Liu, C.; Liu, Y.; Gu, J. Robust solid–solid phase change coating encapsulated glass fiber fabric with electromagnetic interference shielding for thermal management and message encryption. *Adv. Funct. Mater.* **2024,** 34, 2409146.

[179] Zhang, X.; Wang, X.; Lei, Z.; Wang, L.; Tian, M.; Zhu, S.; Xiao, H.; Tang, X.; Qu, L. Flexible MXene-decorated fabric with interwoven conductive networks for integrated joule heating, electromagnetic interference shielding, and strain sensing performances. *ACS Appl. Mater. Interfaces* **2020,** 12, 14459-14467.

[180] Tan, X.; He, Y.; Wang, C.; Zhang, Y.; Wang, W.; Li, H.; Yu, R. Hierarchical mxene/$Fe_3O_4$/cellulose nanofiber composites with layer-by-layer architecture for high-performance electromagnetic interference shielding. *Compos. Sci. Technol.* **2025,** 265, 111136.

[181] Sobolčiak, P.; Ali, A.; Hassan, M.K.; Helal, M.I.; Tanvir, A.; Popelka, A.; Al-Maadeed, M.A.; Krupa, I.; Mahmoud, K.A. 2D $Ti_3C_2T_x$ (MXene)-reinforced polyvinyl alcohol (PVA) nanofibers with enhanced mechanical and electrical properties. *Plos One* **2017,** 12, e0183705.

[182] Eom, W.; Shin, H.; Ambade, R.B.; Lee, S.H.; Lee, K.H.; Kang, D.J.; Han, T.H. Large-scale wet-spinning of highly electroconductive MXene fibers. *Nat. Commun.* **2020,** 11, 2825.

[183] Zhang, J.Z.; Uzun, S.; Seyedin, S.; Lynch, P.A.; Akuzum, B.; Wang, Z.Y.; Qin, S.; Alhabeb, M.; Shuck, C.E.; Lei, W.W.; Kumbur, E.C.; Yang, W.R.; Wang, X.A.; Dion, G.; Razal, J.M.; Gogotsi, Y. Additive-free MXene liquid crystals and fibers. *ACS Cent. Sci.* **2020,** 6, 254-265.

[184] He, M.; Lv, X.; Peng, H.; Zhou, Y.; Li, H.; Li, Z.; Wang, Y.; Bu, X. Biomimetic artificial nacre-like microfiber of Co/C modified cellulose nanofiber/$Ti_3C_2T_x$ MXene with efficient microwave absorption. *Chem. Eng. J.* **2024,** 491, 151726.

[185] Soomro, R.A.; Zhang, P.; Fan, B.M.; Wei, Y.; Xu, B. Progression in the oxidation stability of MXenes. *Nano-Micro Lett.* **2023,** 15, 108.

[186] Kedambaimoole, V.; Harsh, K.; Rajanna, K.; Sen, P.; Nayak, M.M.; Kumar, S. MXene wearables: properties, fabrication strategies, sensing mechanism and applications. *Mater. Adv.* **2022,** 3, 3784-3808.

[187] Kang, C.S.; Kim, J.K.; Lee, C.S.; Chang, H.J.; Cho, Y.H.; Prasad, C.; Choi, H.Y. Facile fabrication and characterization of MXene/cellulose composites for electrical properties, electric heating performance. *Fash. Text.* **2024,** 11, 1.

[188] Da, Y.; Qu, Q.Q.; Kong, L.; Liu, Q.; Zhu, M.H.; Du, Y.M.; Tian, X.Y.; Liu, Y.Y.; Wang, H. A high-performance, oxidation resistance and flexible Zn@MXene/cellulose nanofibers electromagnetic shielding film. *RSC Adv.* **2023,** 13, 6619-6629.

[189] Han, M.; Shen, W.; Corriou, J.-P. Polydopamine-modified MXene/cellulose nanofibers composite film for self-powered humidity sensing and humidity actuating. *Nano Energy* **2024,** 123, 109445.

[190] Zhou, Y.; Zhang, Y.; Pang, Y.; Guo, H.; Guo, Y.; Li, M.; Shi, X.; Gu, J. Thermally conductive $Ti_3C_2T_x$ fibers with superior electrical conductivity. *Nano-Micro Lett.* **2025,** 17, 235.

[191] Cao, W.T.; Ma, C.; Tan, S.; Ma, M.G.; Wan, P.B.; Chen, F. Ultrathin and flexible CNTs/MXene/cellulose nanofibrils composite paper for electromagnetic interference shielding. *Nano-Micro Lett.* **2019,** 11, 72.

[192] Li, J.; Xu, L.; Pan, H.; Wang, L.; Liu, Y.; Shen, Y. Flexible superhydrophobic fabric with electromagnetic interference shielding based on MXene and cellulose nanofibers. *J. Porous Mater.* **2024,** 31, 945-957.

[193] Feng, S.; Yi, Y.; Chen, B.; Deng, P.; Zhou, Z.; Lu, C. Rheology-guided assembly of a highly aligned MXene/cellulose nanofiber composite film for high-performance electromagnetic interference shielding and infrared stealth. *ACS Appl. Mater. Interfaces.* **2022,** 14, 36060-36070.

[194] Feng, S.Y.; Zhan, Z.Y.; Yi, Y.; Zhou, Z.H.; Lu, C.H. Facile fabrication of MXene/cellulose fiber composite film with homogeneous and aligned structure via wet co-milling for enhancing electromagnetic interference shielding performance. *Compos. Part A* **2022,** 157, 106907.

[195] Zhao, H.; Gao, T.; Yun, J.; Chen, L. Robust liquid metal reinforced cellulose nanofiber/MXene composite film with Janus structure for electromagnetic interference shielding and electro-/photothermal conversion applications. *J. Mater. Sci. Technol.* **2024,** 191, 23-32.

[196] Zhang, S.; Wu, J.; Hou, Z.-L.; Hu, P.; Cai, B.; Liang, C.; Zhou, L.; Liang, W.; Xue, Y.; Koo, M.C.; Zhao, P.-Y.; Liu, L.-M.; Liu, M.; Wang, G.-S. Regular-wrinkling tunable MXene lattice for

electromagnetic interference shielding. *Nat. Commun.* **2026,** 17, 1275.

[197] Liu, Q.; Li, C.; Ji, X.X.; Chen, L.; Lang, J.Q.; Ma, M.G. Preparation of excellent flame retardant system for high-performance triboelectric nanogenerators using electrospinning and two-step coating methods. *Chem. Eng. J.* **2025,** 525, 170531.

[198] Tao, W.; Shao, W.; Ma, M.; Chen, S.; Shi, Y.; He, H.; Zhu, Y.; Wang, X. Ag anchored mesoporous carbon hollow sphere in Cellulose nanofibers/MXene composite films for high-performance electromagnetic interference shielding. *Nano Mater. Sci.* **2025,** 7, 65-73.

[199] Feng, M.; Feng, S.; Yu, T.; Zhu, S.; Cai, H.; He, X.; Liu, Y.; He, M.; Bu, X.; Huang, J.; Zhou, Y. Versatile and comfortable janus fabrics for switchable personal thermal management and electromagnetic interference shielding. *Adv. Fiber Mater.* **2024,** 6, 911-924.

[200] Li, S.; Ma, Z.; Wang, L.; Li, X. Toughness and high-electromagnetic-shielding CPM composite film with multilayer sandwich structure based on Mxene. *Adv. Eng. Mater.* **2024,** 26, 2301780.

[201] Guo, Z.; Ren, P.; Yang, F.; Wu, T.; Zhang, L.; Chen, Z.; Ren, F. Robust multifunctional composite films with alternating multilayered architecture for highly efficient electromagnetic interference shielding, Joule heating and infrared stealth. *Compos. Part B Eng.* **2023,** 263, 110863.

[202] Xuan, Q.-F.; Zhao, P.-Y.; Peng, H.; Zhang, S.; Cai, B.; Niu, F.-Y.; Koo, M.C.; Sun, X.-B.; Jiang, X.; Wang, G.-S. Hierarchical modular architecture enabling intelligent dynamic thermal management and superior electromagnetic interference shielding. *Nano-Micro Lett.* **2026,** 18, 290.

[203] Liang, W.; Wu, J.; Zhang, S.; Zhao, P.-Y.; Zuo, X.; Wang, G.-S. Construction of PI-MXene-MWCNT nanocomposite film integrating conductive gradient with sandwich structure for high-efficiency electromagnetic interference shielding in extreme environments. *Carbon.* **2024,** 228, 119328.

[204] Zhou, Z.; Song, Q.; Huang, B.; Feng, S.; Lu, C. Facile fabrication of densely packed $Ti_3C_2$ MXene/nanocellulose composite films for enhancing electromagnetic interference shielding and electro-/photothermal performance. *ACS Nano.* **2021,** 15, 12405-12417.

[205] Chu, Q.; Tao, W.; Lin, H.; Ma, M.; Chen, S.; Shi, Y.; He, H.; Wang, X. Well-designed structure of sandwich-like composite films based on hollow polyaniline and MXene with enhanced electromagnetic wave absorption. *Ind. Crop. Prod.* **2023,** 194, 116299.

[206] Jin, X.; Wang, J.; Dai, L.; Liu, X.; Li, L.; Yang, Y.; Cao, Y.; Wang, W.; Wu, H.; Guo, S. Flame-retardant poly(vinyl alcohol)/MXene multilayered films with outstanding electromagnetic interference shielding and thermal conductive performances. *Chem. Eng. J.* **2020,** 380, 122475.

[207] Wang, Y.; Peng, H.-K.; Li, T.-T.; Shiu, B.-C.; Ren, H.-T.; Zhang, X.; Lou, C.-W.; Lin, J.-H. MXene-coated conductive composite film with ultrathin, flexible, self-cleaning for high-performance electromagnetic interference shielding. *Chem. Eng. J.* **2021,** 412, 128681.

[208] Ma, X.; Shen, B.; Zhang, L.; Chen, Z.; Liu, Y.; Zhai, W.; Zheng, W. Novel straw-derived carbon materials for electromagnetic interference shielding: a waste-to-wealth and sustainable initiative. *ACS Sustainable Chem. Eng.* **2019,** 7, 9663-9670.

[209] Chen, J.; Liu, Y.-l.; Sun, D.-x.; Qi, X.-d.; Yang, J.-h.; Wang, Y. Recent progress in structural design of graphene/polymer porous composites toward electromagnetic interference shielding application. *Chem. Eng. J.* **2024,** 495, 153586.

[210] Gu, Y.; Yu, L.; Mou, J.; Wu, D.; Zhou, P.; Xu, M. Mechanical properties and application analysis of spider silk bionic material. *e-Polymers.* **2020,** 20, 443-457.

[211] Liu, Q.; Zhang, Y.; Liu, Y.; Liu, Z.; Zhang, B.; Zhang, Q. Ultrathin, biomimetic

multifunctional leaf-like silver nanowires/$Ti_3C_2T_x$ MXene/cellulose nanofibrils nanocomposite film for high-performance electromagnetic interference shielding and thermal management. *J. Alloys Compd.* **2021,** 860, 158151.

[212] Wei, J.; He, P.; Yang, Y.; Tang, C.; Long, Z.; Chen, X.; Lei, T.; Dai, L. Enhancing the electromagnetic interference shielding performance of composite paper with corrugated paper-like structure. *Chem. Eng. J.* **2024,** 497, 154969.

[213] Wei, L.; Ren, Y.; Hou, Y.; Jin, P.; Zheng, Y.; Wu, Z. MXene/nanocellulose/carbon sphere composite films with a multistage "egg-box" structure for electromagnetic-interference shielding and pressure sensors. *J. Mater. Chem. A.* **2025,** 13, 8876-8889.

[214] Nouseen, S.; Pumera, M. MXene 3D/4D printing: ink formulation and electrochemical energy storage applications. *Adv. Funct. Mater.* **2025,** 35, 2421987.

[215] Sun, Z.Y.; Han, C.P.; Song, M.M.; Wen, L.; Tian, D.M.; Li, H.B.; Jiang, L. Fabrication of cysteine-responsive biomimetic single nanochannels by a thiol-yne reaction strategy and their application for sensing in urine samples. *Adv. Mater.* **2014,** 26, 455-460.

[216] Mai, T.; Chen, L.; Liu, Q.; Guo, Z.H.; Ma, M.G. Zeolitic imidazolate frameworks derived magnetic nanocage/MXene/nanocellulose bilayer aerogels for low reflection electromagnetic interference shielding and light-to-heat conversion. *Adv. Funct. Mater.* **2025,** 35, 2417947.

[217] Zhang, S.; Liang, C.-M.; Zhou, L.; Wu, J.; Koo, M.C.; Wu, Z.; Chen, Y.-T.; Wang, G.-S. Heterolayered carbonized MXene/polyimide aerogel for low-reflection electromagnetic interference shielding and multi-spectrum compatible protection. *Nano-Micro Lett.* **2026,** 18, 204.

[218] Liang, W.; Wu, J.; Zhang, S.; Zhao, P.-Y.; Cong, Y.; Guo, Y.; Wang, G.-S. Porous $Ti_3C_2T_x$ MXene nanosheets sandwiched between polyimide fiber mats for electromagnetic interference shielding. *Nano Res.* **2024,** 17, 2070-2078.

[219] Zhao, H.; Wang, J.; He, M.; Li, S.; Guo, H.; Kan, D.; Qiu, H.; Chen, L.; Gu, J. Electromagnetic interference shielding films: structure design and prospects. *Small Methods* **2025,** 9, 2401324.

[220] Ma, Z.; Deng, Z.; Zhou, X.; Li, L.; Jiao, C.; Ma, H.; Yu, Z.-Z.; Zhang, H.-B. Multifunctional and magnetic MXene composite aerogels for electromagnetic interference shielding with low reflectivity. *Carbon.* **2023,** 213, 118260.

[221] Jalali, A.; Gupta, T.; Pakharenko, V.; Rejeb, Z.B.; Kheradmandkeysomi, M.; Sain, M.; Park, C.B. Lightweight 3D-printed chitosan/MXene aerogels for advanced electromagnetic shielding, energy harvesting, and thermal management. *Carbohydr. Polym.* **2025,** 352, 123252.

[222] Jin, X.; Li, L.; Zhao, S.; Li, X.; Jiang, K.; Wang, L.; Shen, G. Assessment of occlusal force and local gas release using degradable bacterial cellulose/$Ti_3C_2T_x$ MXene bioaerogel for oral healthcare. *ACS Nano* **2021,** 15, 18385-18393.

[223] Bi, X.; Li, M.; Zhou, G.; Liu, C.; Huang, R.; Shi, Y.; Xu, B.B.; Guo, Z.; Fan, W.; Algadi, H.; Ge, S. High-performance flexible all-solid-state asymmetric supercapacitors based on binder-free MXene/cellulose nanofiber anode and carbon cloth/polyaniline cathode. *Nano Res.* **2023,** 16, 7696-7709.

[224] Shi, Y.; Zhu, Y.; Liu, S.; Fu, L.; Chen, J.; Liu, J.; Tang, L.; Gao, J.; Song, P. Multi-hierarchically constructing durable and flame retardant CNF/MXene/PDMS composite aerogels for superhigh electromagnetic shielding performance and ultralow thermal conductivity. *Small* **2025,** 21, 2500556.

[225] Chen, L.; Mai, T.; Ji, X.-X.; Wang, P.-L.; Qi, M.-Y.; Liu, Q.; Ding, Y.; Ma, M.-G. 3D printing

of customizable and lightweight multilayer MXene/nanocellulose architectures for tunable electromagnetic interference shielding via direct ink writing. *Chem. Eng. J.* **2023,** 476, 146652.

[226] Ahmed, B.; Hossain, M.J.; Al Parvez, A.; Talukder, A.; Al-Amin, M.; Al Mahmud, M.A.; Islam, T. Recent Advancements of MXene/nanocellulose-based hydrogel and aerogel: a review. *Adv. Energy Sustain. Res.* **2024,** 5, 2300231.

[227] Zhang, R.; Xie, D.; Zhang, C.; Xu, Z.; Fang, Y.; Wang, W.; Xu, M.; Song, Y. A highly stretchable, self-adhesive, anti-freezing, and highly sensitive dual-network conductive hydrogel sensor for multifunctional electronic skin. *J. Mater. Chem. A.* **2023,** 11, 24608-24617.

[228] Chen, L.; Yang, S.-C.; Liu, Q.; Lang, J.-Q.; Ma, M.-G. Bioinspired by staggered cellular structures: 3D-printed aerogel frameworks for ink rheological, parametric optimization, and enhanced terahertz electromagnetic shielding performance. *Nano Res.* **2026,** 19, 94908105.

[229] Amani, A.M.; Tayebi, L.; Vafa, E.; Abbasi, M.; Vaez, A.; Kamyab, H.; Chelliapan, S.; Azizli, M.J.; Bazargan-Lari, R. On the horizon of greener pathways to travel into a greener future portal: Green MXenes, environment-friendly synthesis, and their innovative applications. *J. Cleaner Prod.* **2024,** 436, 140606.

[230] Hu, W.; Yang, M.; Fan, T.; Li, Z.; Wang, Y.; Li, H.; Zhu, G.; Li, J.; Jin, H.; Yu, L. A simple, efficient, fluorine-free synthesis method of MXene/$Ti_3C_2T_x$ anode through molten salt etching for sodium-ion batteries. *Battery Energy* **2023,** 2, 20230021.

[231] Guo, J.; Zhang, T.; Hao, X.; Liu, S.; Zou, Y.; Li, J.; Wu, W.; Chen, L.; Liu, X. Aramid nanofiber/MXene-reinforced polyelectrolyte hydrogels for absorption-dominated electromagnetic interference shielding and wearable sensing. *Nano-Micro Lett.* **2025,** 17, 271.

[232] Durmaz, B.U.; Salman, A.O.; Aytac, A. Electromagnetic interference shielding performances of carbon-fiber-reinforced PA11/PLA composites in the x-band frequency range. *ACS Omega* **2023,** 8, 22762-22773.

[233] Wei, J.; Dai, L.; He, P.; Zhu, M.; Jiang, F.; Zhou, Z.; Fei, G.; Lei, T. Ultrathin and flexible MXene-contained electromagnetic interference shielding composite paper designed with a protective hydrogel film. *J Mater Sci. Technol.* **2024,** 169, 199-208.

[234] Fazlalizadeh, F.; Nezafat, Z.; Javanshir, S.; Peymanfar, R. Rational design of microwave absorbing cryogels using microcrystalline cellulose and cellulose-derived nutshell/metal nanoparticles. *Ind. Crop. Prod.* **2025,** 229, 120954.

[235] Selseleh-Zakerin, E.; Mirkhan, A.; Shafiee, M.; Alihoseini, M.; Khani, M.; Shokri, B.; Tavassoli, S.H.; Peymanfar, R. Plasma engineering toward improving the microwave-absorbing/shielding feature of a biomass-derived material. *Langmuir* **2024,** 40, 12148-12158.

[236] Liu, A.; Zhang, Y.; Xu, X.; Kong, J.; Gu, J. Multi-field synergy for orchestrating filler angles in polyimide aerogels with switchable electromagnetic interference shielding. *Adv. Mater.* **2026,** 6, 10.1002/adma.73267.

[237] Tang, J.; Gao, Y.; Li, T.; Qin, R.; Qi, Q.; Meng, F. Thermoresistive network in phase-transition hydrogel: achieving on/off switchable electromagnetic interference shielding. *Adv. Funct. Mater.* **2025,** 35, 2504959.